

5. CURRENT ENGINEERED BARRIER SYSTEM DESIGN

5.1 INTRODUCTION

Section 5 provides a context for Engineered Barrier System (EBS) analogues that are discussed in Sections 6 and 7. This section summarizes the key components of the EBS system and describes the materials proposed to be used in the construction of these components. Finally, the key processes that are expected to occur during the operational life span of the EBS are described.

5.2 EBS COMPONENTS

The EBS currently planned for the potential Yucca Mountain repository (Figure 5-1) consists of three main components: (1) drip shield, (2) emplacement drift invert, and (3) waste package (DOE 2001 [153849], Section 2.4). Because they will affect the performance of the EBS, materials included within the waste forms and used in the construction of the emplacement drifts also are considered in the evaluation of the EBS. The following summary of the components of the EBS system is based upon Sections 2.4 and 3 of the *Yucca Mountain Science and Engineering Report* (S&ER) (DOE 2001 [153849]).

5.2.1 Drip Shield

The drip shield is designed to serve as a protective barrier, for the length of emplacement drifts, that will divert water dripping from the drift walls, thus minimizing direct dripping onto the waste packages. The drip shield has the added function of protecting the waste package from rock falls from the drift perimeter. These functions require that the drip shield assembly is both highly resistant to corrosion and has the structural strength to withstand rock falls.

The drip shield consists of three separate elements: the drip shield, supporting structural members, and stands (or “feet”) upon which the shield assembly rests (Figure 5-2). Current design plans call for the drip shield to be manufactured from 15 mm (0.6 in.) thick Titanium Grade 7 plates for long-term corrosion resistance. The structural members will be constructed using Titanium Grade 24, which has greater strength than Titanium Grade 7. Alloy 22 (see Table 5.2) will be used for the feet, preventing direct contact between the titanium structural members and the carbon steel beams of the invert.

5.2.2 Drift Invert

The drift invert is designed to form a stable, level platform along the base of the emplacement drift on which the waste package and drip-shield assemblies will be placed. The invert as currently planned (DOE 2001 [153849], Section 2.4.1) consists of two components: a steel invert structure and a crushed-tuff invert ballast.

The steel invert structure needs to provide sufficient support for all expected pre-closure activities for up to 300 years and must also keep the waste packages in a horizontal position for 10,000 years after closure. The steel structure consists of transverse and longitudinal support beams, which serve to transfer the weight of the waste package and drip shield (along with any

needed emplacement and maintenance equipment during the initial phases of operation) to the bedrock (Figure 5-3). Gantry rails, needed to transport the waste packages and drip shields into the tunnel, will be placed along the margins of the support beam structure. Guide beams will be used (if considered necessary to mitigate movement resulting from seismic events) to secure the waste package emplacement pallets and the drip shield assembly. The current design calls for the invert support and guide beams to be manufactured of ASTM A 572/A 572M steel, which was chosen to provide sufficient strength for the emplacement drift environment. The gantry rail will be made of ASTM A 759 carbon steel (DOE 2001 [153849], Section 2.4.1.1).

The invert ballast is designed so that moisture present in the emplacement drift will drain directly into the surrounding rock without flowing along the base of the drift. Crushed tuff, produced by crushing material obtained during the excavation of the emplacement drifts, would be used as the primary ballast material. The ballast will be placed around the steel invert beams, to a level just below the top of the support beams, so that the waste package pallets and drip shields rest on the support beams and not on the ballast. The ballast material will be compacted so that no significant settling will occur over time. The crushed tuff should not be affected by heating related to emplacement of the waste packages. Transport of radionuclides within the crushed tuff is expected to be dominated by diffusive transport, thus serving to retard any potential release of radionuclides into the surrounding host rocks (DOE 2001 [153849], Section 2.4.1.2).

5.2.3 Waste Package

The waste package assembly is designed to securely contain high-level radioactive wastes and serve as the primary element to the EBS. The waste package system consists of two main components: a waste package emplacement pallet and a sealed, corrosion-resistant waste package canister (Figure 5-4).

The waste package emplacement pallets are designed to support the waste package canisters in a horizontal position and facilitate line-loading of the waste packages. Current plans call for the pallets to be manufactured from plates of Alloy 22 (a material highly resistant to corrosion) with support tubes fabricated from Stainless Steel Type 316L (DOE 2001 [153849], Section 2.4.3.1). The V-shaped design will allow the pallets to be used for all waste package canisters.

A number of distinct waste package designs have been developed to accommodate the different waste forms generated from boiling water and pressurized water reactors, excess weapons material, high-level waste, and DOE and naval spent nuclear fuel (Figure 5-5). All of these waste package designs contain a number of important components that are needed to meet performance criteria. The performance criteria (DOE 2001 [153849], Section 3.4.1) are as follows:

- Strength
- Resistance to corrosion and microbial attack
- Predictable materials behavior
- Compatibility with waste package and waste form materials
- Ease of fabrication
- Proven performance record
- Favorable heat transfer properties
- Utility in shielding and preventing criticality.

Table 5-1 lists the major waste package components for commercial spent nuclear fuel waste packages, the composition of each component, and the component function(s).

The different materials chosen for the construction of the waste package system are based on the functional requirements for each component. Key properties include resistance to corrosion and cracking caused by thermal, mechanical, and chemical processes; preservation of the structural integrity of the waste package system; conduction of heat away from the waste forms; and the ability to prevent criticality from occurring. A brief description of each of the main types of materials incorporated in the current design (DOE 2001 [153849], Section 3) is given below.

5.2.3.1 Corrosion-Resistant and Structural Materials

Alloy 22 was selected for the outer barrier of the waste package because of its resistance to corrosion under conditions of high temperatures and low humidity and under all low-temperature conditions, its similar thermal expansion coefficient to stainless steel, and because it can be welded more easily than can titanium. The chemical composition of Alloy 22 is given in Table 5-2. Stainless Steel Type 316NG was chosen for the inner cylinder of the waste package because of its relative strength, compatibility with Alloy 22, and its affordability. The chemical composition of Stainless Steel Type 316NG is given in Table 5-3.

5.2.3.2 Other Waste Package Materials

A variety of other materials will be used in the fabrication of the waste package assembly (DOE 2001 [153849], Section 3.2.2.1). These include Neutronit A 978 (borated 316 stainless steel) or SA 516 Grade 70 carbon steel plates, boron carbide rods with Zircaloy cladding used for control of criticality within the waste package container, and aluminum shunts (SB-209 6061 T4) to assist in heat transport away from the waste form. The waste package will encompass the waste form materials described in Section 5.2.4.

5.2.4 Waste Form Components

The waste forms for disposal at the potential Yucca Mountain repository include spent fuel from commercial power reactors and that owned by the U.S. Department of Energy, solidified high-level radioactive waste, and plutonium waste from excess nuclear weapons. All waste must be in solid form and must not contain flammable or chemically reactive materials. The waste forms will contain fuel rods constructed out of Zircaloy and stainless steel as well as a variety of radioactive waste types, including uranium metal, uranium oxide, uranium dioxide, radioactive borosilicate glass, and plutonium encased in ceramic pellets (DOE 2001 [153849], Section 3). Analogues to waste form materials and their degradation are discussed in Section 4.

5.2.5 Emplacement Drifts

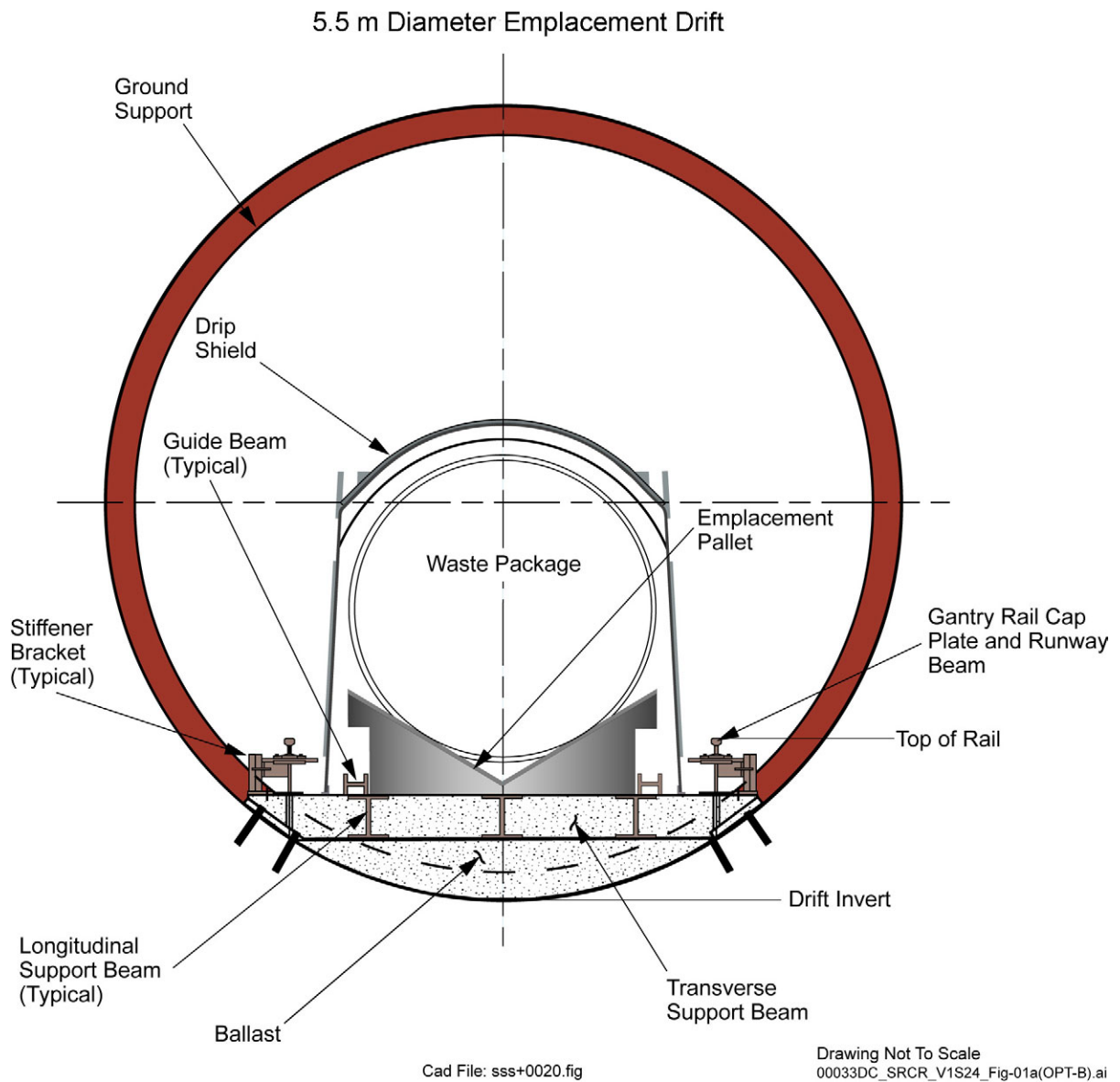
While the emplacement drifts are not considered a component of the engineered barrier system, the materials used in their construction could significantly affect the EBS performance. The emplacement drifts contain a variety of materials that are used to help maintain the integrity of the drift after excavation. The ground support system, designed to stabilize the emplacement drift, includes W6X20 rolled steel ring beams (steel sets), tie rods, welded wire fabric, rock bolts,

and cementitious grout used to secure the rock bolts in place (DOE 2001 [153849], Section 2.3.4.1.2.1). Analogues relevant to emplacement drift components are discussed in Section 7.

5.3 PROCESSES AFFECTING EBS PERFORMANCE

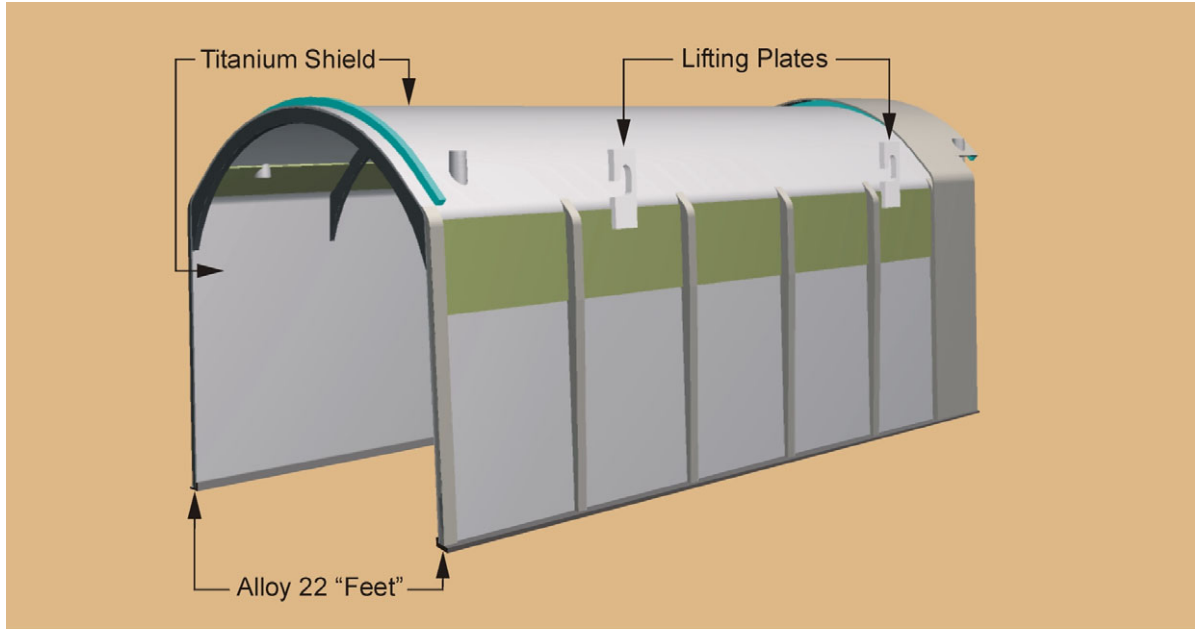
Numerous processes and event scenarios have been identified and considered in designing the EBS (DOE 2001 [153849], Sections 2.4 and 3.1). These can be grouped into four major categories: structural, thermal, chemical, and nuclear criticality. The structural events evaluated involve scenarios (such as mishandling of the packages, seismic events, or rock falls) that would result in the waste package being physically disturbed by an impact that could potentially result in breaching the sealed waste packages. Thermal processes include changes in physical and chemical properties associated with heating caused by radioactive decay of the waste forms, such as thermal expansion and cracking, as well as the effects of heat transfer properties. Chemical processes such as corrosion and chemical reaction of the different materials could also result in breaching of the sealed waste packages and subsequent release of radionuclides into the surrounding environment. Special attention has been placed on the design of the waste packages and composition of the waste forms to prevent the radioactive waste from achieving criticality. The selection of the different materials used in construction of the EBS components has been made to ensure the long-term structural, thermal, and chemical integrity of the waste packages and to prevent the waste forms from going critical.

While the properties of all of the materials selected for the EBS design have been extensively tested and determined in the laboratory, the long-term performance of these materials under the predicted temperature, humidity and chemical environment for the potential Yucca Mountain repository has not been experimentally confirmed. Natural analogues for similar materials found in the natural environment can be used to validate long-term performance models for the EBS. The following sections (6 and 7) provide descriptions of natural analogues for waste package materials and for processes that might take place within the EBS.



Source: DOE 2001 ([153849], Figure 2-71).

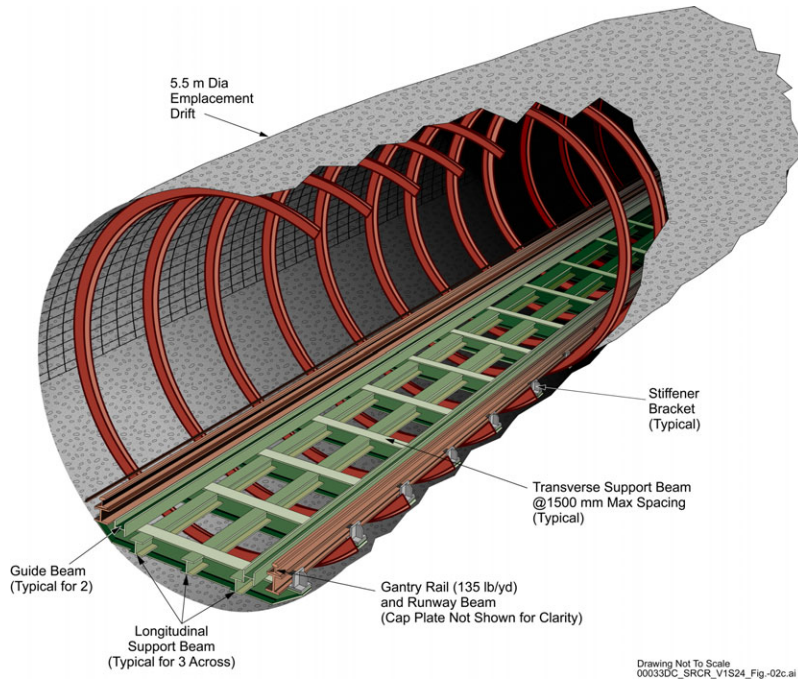
Figure 5-1. Cross Section of Emplacement Drift with EBS Components



Drawing Not To Scale
00033DC_ATP_Z1S24_Fig-03a.cdr

Source: DOE 2001 ([153849], Figure 2-73).

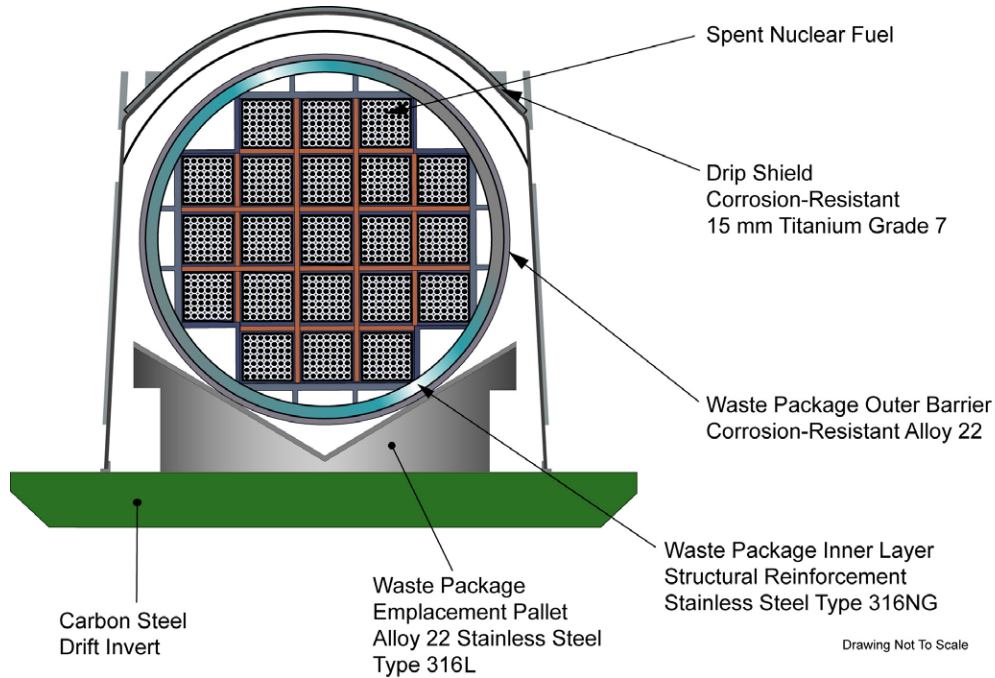
Figure 5-2. Schematic View of Drip Shield Assembly with Drip Shield, Support Members, and Feet



Drawing Not To Scale
00033DC_SRCR_V1S24_Fig-02c.ai

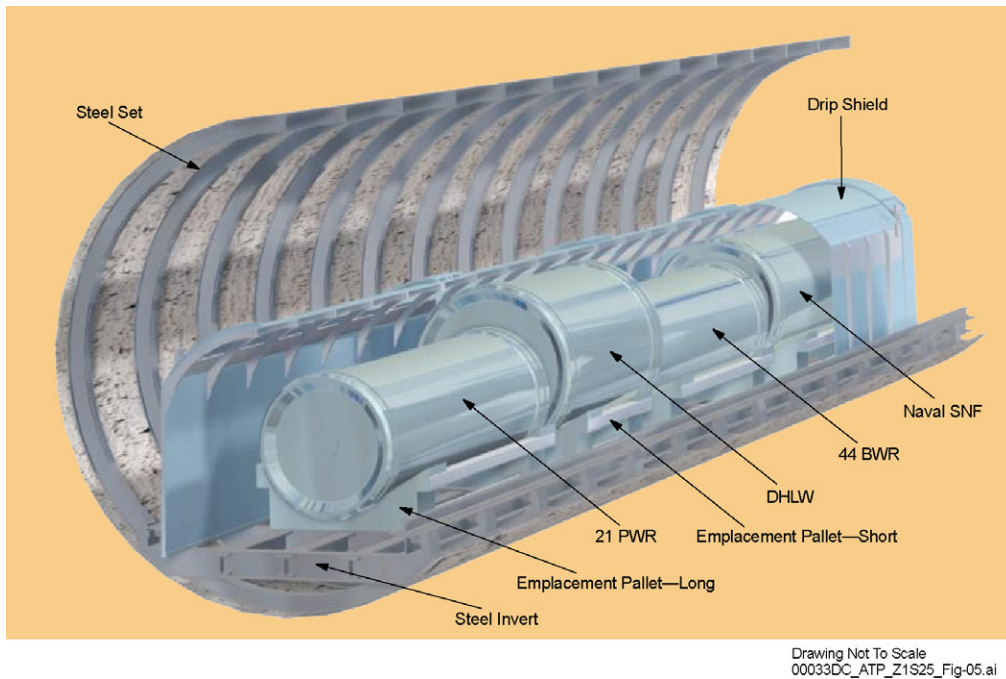
Source: DOE 2001 ([153849], Figure 2-72).

Figure 5-3. Perspective View of Steel Invert Structure in Emplacement Drift



Source: DOE 2001 ([153849], modified from Figure 3-1).

Figure 5-4. Cross Section of Waste Package, Emplacement Pallet, and Drip Shield



NOTE: PWR = Pressurized Water Reactor; DHLW = Defense High-Level Radioactive Waste; BWR = Boiling Water Reactor; and SNF = Spent Nuclear Fuel. Source: DOE 2001 ([153849], Figure 2-77).

Figure 5-5. Schematic View of Different Waste Packages in Emplacement Drift

Table 5-1. Commercial Spent Nuclear Fuel Waste Package

Component	Composition	Function
Outer barrier and lids	Alloy 22	Protect against corrosion
Support ring	Alloy 22	Hold inner cylinder in place
Inner structural shell and lid	Stainless Steel Type 316NG	Provide structural integrity
Waste package fill gas	Helium	Heat conductor, with need to be compatible with spent fuel
Fuel tubes for internal basket	Carbon steel (SA 516 Grade 70)	Hold fuel assemblies in place and provide structural strength and conduct heat away from cladding
Interlocking plates for internal basket	Carbon steel (SA 516 Grade 70)	Provide structural strength to maintain fuel geometry and prevent criticality
Neutron absorber materials for internal basket	Neutronic A 978 (borated 316 stainless steel)	Prevent criticality, provides structural strength and conduct heat away from waste form to walls of waste package
Thermal shunts for internal basket	Aluminum alloy (SB-209 6061 T4)	Transfer heat from waste form to walls of waste package
Structural guides for internal basket	Carbon steel (SA 516 Grade 70)	Provide structural strength to hold basket structure in place and prevent criticality, conduct heat to walls of waste package
Control rods	Boron carbide with Zircaloy cladding	Provide long-term criticality control

Source: DOE 2001 [153849], modified from Table 3-9, Sections 3.1 and 3.2.2.

Table 5-2. Chemical Composition of Alloy 22

Element	Composition (wt %)
Nickel	50 to 63
Chromium	20.0 to 22.5
Molybdenum	12.5 to 14.5
Iron	2.0 to 6.0
Tungsten	2.5 to 3.5
Cobalt	2.50 (max)
Manganese	0.50 (max)
Vanadium	0.35 (max)
Silicon	0.08 (max)
Phosphorus	0.02 (max)
Sulfur	0.02 (max)
Carbon	0.015 (max)

Source: DOE 2001 [153849], modified from Table 3-12.

Table 5-3. Chemical Composition of Stainless Steel Type 316NG

Element	Composition (wt %)
Iron	61 to 71
Chromium	16.00 to 18.00
Nickel	11.00 to 14.00
Molybdenum	2.00 to 3.00
Manganese	2.00 (max)
Silicon	0.75 (max)
Copper	0.50 (max)
Cobalt	0.10 (max)
Vanadium	0.1 (max)
Nitrogen	0.06 to 0.10
Titanium	0.05 (max)
Tantalum and Niobium	0.05 (max)
Aluminum	0.04 (max)
Phosphorus	0.030 (max)
Carbon	0.020 (max)
Bismuth + Tin + Arsenic + Lead + Antimony + Selenium	0.02 (max)
Sulfur	0.005 (max)
Boron	0.002 (max)

Source: DOE 2001 [153849], modified from Table 3-13.

6. WASTE PACKAGE DEGRADATION ANALOGUES

6.1 INTRODUCTION

This section describes the use of natural analogues to evaluate the long-term performance of metals used in the fabrication of waste packages for storage of high-level radioactive waste. Key concerns for the waste package materials (described in Section 5) include the possible degradation and corrosion of metals caused by mechanical stress, hostile physical and chemical environments, and metallurgical factors. The primary degradation and corrosion issues expected for Yucca Mountain include elevated temperature and humidity, and contact with seepage water that could have corrosive chemistry. A number of different analogues were previously discussed in Chapter 13 of the *Yucca Mountain Site Description* (CRWMS M&O 2000 [151945], Section 13.3.5); those analogues applicable to the waste materials described in Section 5 are briefly summarized below. Additional analogue examples are discussed in more detail in the following subsections.

The long-term stability of the waste package materials is directly related to repository environmental conditions. Preservation of delicate archaeological materials, including metals, appears to be enhanced by their location in an arid or semi-arid unsaturated environment (CRWMS M&O 2000 [151945], Section 13.3.4). Mummified remains 4,000 to 8,000 years in age were recently discovered in shallow burial pits in the high Andes Mountains of Chile. The Dead Sea scrolls were preserved in caves along the shores of the Dead Sea for over 2,000 years. All of these artifacts have survived millennia, and their preservation is attributed in part to being in arid to semiarid unsaturated environments (Winograd 1986 [127015], p. 8).

Metal analogues, involving both naturally occurring and archaeological objects, were also described in the *Yucca Mountain Site Description* (CRWMS M&O 2000 [151945], Section 13.3.5). A cache of Roman iron nails was recovered after almost 1,900 years of burial in Scotland (Miller et al. 1994 [126089], pp. 114–119). Corrosion of the outermost nails formed a protective rust rind, serving to create a more reducing (and thus more stable) environment for the innermost nails. Using a variety of iron archaeological artifacts, Johnson and Francis (1980 [125291], Fig. 3-1) calculated general corrosion rates of 0.1 to 10 $\mu\text{m}/\text{yr}$ for most of the artifacts under a range of environmental conditions. Iron meteorites often have poorly constrained exposure histories, but differential corrosion of different mineral phases can be used to estimate relative resistance to corrosion, suggesting that Ni-rich phases (taenite and schreibersite) are more stable than Fe-rich phases (Johnson and Francis 1980 [125291], p. 4.23). Copper-bearing archaeological artifacts, such as sunken and buried bronze cannons, can also be used to estimate general corrosion rates over extended (hundreds to thousands of years) periods of time. These metal analogues, while differing in chemical composition from the waste package films, provide important insights into the way different metals survive corrosion over long time periods, and illustrate the importance of passive films.

Most of the metals being considered for use in the waste packages at a potential Yucca Mountain repository consist of alloys that do not occur naturally and are not present in the archaeological record (see Tables 5-1 to 5-3). However, the long-term behavior of metals with similar compositions that are present either as minerals or as man-made objects can be used to build

confidence in long-term performance models of the waste package materials. Analogues to long-term behavior of metals related to waste package materials are described in Section 6.2.3. Information found in Section 6.2 may help to support arguments associated with Key Technical Issue (KTI) KUZ0407 listed in Table 1-1.

6.2 NATURAL ANALOGUE STUDIES OF CORROSION

This section will discuss new work on some of the natural analogues previously summarized in Chapter 13 of the *Yucca Mountain Site Description* (CRWMS M&O 2000 [151945]), as well as present information on examples not previously discussed in the Site Description.

6.2.1 Environmental Factors Related to Corrosion

Knowledge of the in-drift physical and chemical environment at Yucca Mountain is critical in predicting the long-term performance of waste packages and the EBS. Processes such as the evaporation and condensation of water, precipitation and dissolution of salts, seepage and mass transport of materials into the drift environment, and the abundance, compositions, and reactions between solid, liquid, and gas phases will affect the physical and chemical integrity of waste packages and other EBS components.

One of the key attributes of the potential Yucca Mountain repository is its location within the unsaturated zone, thus reducing the amount of water that can come into contact with waste packages. Previous reviews of natural analogues of caves within the unsaturated zone have demonstrated that very old archaeological artifacts can be preserved in such environments (CRWMS M&O 2000 [151945], Section 13.3.4). Hundreds of wooden and reed fragments of dart and arrow shafts (dated between 3,300 to 9,300 years B.P.) have been recovered from Pintwater Cave in southern Nevada (Buck and DuBarton 1994 [157438], pp. 228, 239). These delicate items were collected from the limestone cave floor and in a test pit excavated within eolian sediments lining the floor of Pintwater Cave (Buck and DuBarton 1994 [157438], p. 226), and their preservation suggests that they were not subjected to prolonged exposure to water. However, as shown in the following example, the maintenance of a stable microclimate is a critical feature in making caves suitable for long-term preservation.

The Altamira cave, located in northern Spain, is the site of Paleolithic cave paintings (Sanchez-Moral et al. 1999 [157382]). Since the discovery of the prehistoric cave art in 1879, significant degradation of the cave paintings has occurred, leading to the cave being closed to the public in 1977. The cave was reopened in 1982 with fixed limits on the number of visitors. Continuous monitoring of the Altamira cave microclimate within Polychromes Hall (a cave chamber with famous polychromatic paintings) during 1997–1998 determined that increases in temperature ($\Delta = +0.25^\circ\text{C}$) and CO_2 concentrations ($\Delta = +500$ ppmv) resulted directly from the presence of visitors in the cave (Sanchez-Moral et al. 1999 [157382], p. 78).

Sanchez-Moral et al. (1999 [157382]) used these data to estimate effective calcite corrosion rates for both the baseline and modified (visitor-related case) cave conditions. They predicted that the visitor-induced temperature increase (resulting from radiation of body heat) will greatly increase the amount of water condensation occurring on the cave walls and ceiling. The elevated P_{CO_2} (partial pressure of carbon dioxide) conditions caused by human respiration, combined with the

higher amounts of condensation, were predicted to result in visitor-induced corrosion rates (314 mm³/yr) in Polychromes Hall that are 78 times higher than the baseline (no visitor) case

(Sanchez-Moral et al. 1999 [157382], p. 78). As noted by visual observation and modeling, the relatively minor changes in temperature and P_{CO_2} at Altamira had a significant impact on deterioration of the cave art. Thus, the corrosion-resistance properties of waste package materials at Yucca Mountain need to be evaluated for all possible variations in environmental conditions during the postclosure period.

One critical factor affecting the chemical integrity of the waste packages is the potential development of hypersaline fluids within emplacement drifts at Yucca Mountain. Such fluids could be generated by evaporative concentration of dissolved salts in pore waters in the near-drift environment caused by heating, or by dissolution of previously formed salts in the dryout zone around the drift by downward percolating condensate waters and/or surface infiltration. The amount and salinity of water in contact with waste packages depend on a number of factors, including evaporation, condensation, temperature, and fluid flux rates into the emplacement drifts (Figure 6-1). Conceptual and numerical models of these processes suggest that fluid compositions within the emplacement drifts may be highly variable over time (Walton 1994 [127454], pp. 3483–3486).

To constrain models involving the generation of hypersaline fluids at Yucca Mountain, Rosenberg et al. (2001 [154862]) conducted a series of experiments at sub-boiling temperatures (75–85°C) to evaluate the evaporative chemical evolution of pore water from the unsaturated zone and of well water from the saturated zone at Yucca Mountain. Synthetic solutions of these two fluid types were evaporated, with samples collected and analyzed after approximately 100 and 1,000 × evaporative concentration and evaporation to dryness (Table 6-1). A number of different minerals formed from complete evaporation of these waters, including amorphous silica, aragonite, calcite, halite, niter, smectite, thermonatrite, tachyhydrite, and gypsum. The groundwater (obtained from the J-13 well at Yucca Mountain) composition evolved into a high pH, sodium carbonate-bicarbonate brine resulting from the precipitation of calcium-magnesium carbonate, while the UZ pore-water composition evolved into a near-neutral pH, sodium-potassium-calcium-magnesium-chloride-nitrate brine resulting from the precipitation of gypsum. Different fluid chemistry may develop under higher temperature (boiling) conditions as a result of CO_2 degassing, which could have an important impact on the pH of the evolved fluids. These experimental results provide a data set against which to compare brines from analogue sites that have interacted with metals in a natural environment.

Hypersaline fluids, such as those encountered at the Salton Sea geothermal field (Table 6-2), have been observed to aggressively corrode many steel compositions (McCright et al. 1980 [157384], pp. 646–648). Carbon steel drill casings initially used in geothermal production wells at the Salton Sea field experienced general corrosion rates as high as 25.4 mm/yr, with even higher localized corrosion rates observed (Pye et al. 1989 [157385], p. 260). These rates are much higher than the rates of 10–40 $\mu\text{m}/\text{yr}$ obtained by Ahn and Soo (1995 [104751], p. 475) for corrosion tests of A216-Grade WCA low-carbon steel in concentrated synthetic groundwater solutions. The differences in corrosion rates likely result from: (1) differences in steel compositions; (2) higher temperatures for the Salton Sea fluids (232–315°C) than that those used for the corrosion experiments (80–150°C); and (3) much higher salinities for the Salton Sea brines (150,000–300,000 ppm TDS) relative to the synthetic experimental brines (7,455 ppm TDS). Corrosion problems at the Salton Sea were successfully mitigated through the use of a corrosion-resistant titanium alloy (see Section 7.2.1). The current drip shield design for Yucca

Mountain (see Section 5.2.1) calls for the use of titanium because of its corrosion-resistant properties.

Another concern for waste package materials is the possible evaporative concentration of minor dissolved constituents, such as arsenic, lead, and mercury, that could enhance corrosion (BSC 2001 [155950], Section 7.3.1.3.4; [157151], Appendix E, Section 3.1.2). The hypersaline Salton Sea brines have significant concentrations of arsenic (8 ppm) and lead (66 ppm). However, groundwaters in the vicinity of Yucca Mountain have only trace amounts of lead, with a median concentration of 9 ppb (Lee 2001 [155241]; Perfect et al. 1995 [101053]). Two samples of J-13 well water from Yucca Mountain were analyzed for lead, with one sample yielding a value of 3 ppb, while the other was below detection (BSC 2001 [155950], Section 7.3.1.3.4; Perfect et al. 1995 [101053]). Lead concentrations in groundwater at Yucca Mountain may be limited by precipitation of lead in the form of carbonate, oxide, or sulfide minerals, or by sorption onto mineral surfaces (BSC 2001 [155950], Section 7.3.1.3.4, [157151], Appendix E, Section 3.1.2). Evaporative concentration of water in the near-drift environment at Yucca Mountain could result in higher lead concentrations. However, even a 1,000-fold increase in lead concentration in J-13 water would still only result in a brine with ~3 ppm lead, over 20 times lower than the concentrations observed in Salton Sea brines. Thus, the very low concentrations of lead in groundwater at Yucca Mountain greatly reduce the risk that lead (and other trace metals) could pose to the chemical integrity of the waste packages.

6.2.2 Passive Film Formation

The formation of passive films has a significant impact on the corrosion-resistant properties of metals and metal alloys (BSC 2001 [155950], Section 7.3.4). Passive films are stratified coatings consisting of an inner oxide layer and an outer layer of hydroxide or oxyhydroxide (Macdonald 1992 [154720], pp. 3434–3437; Marcus and Maurice 2000 [154738], pp. 145–152). The inner layer forms a corrosion barrier, while exchange occurs within the outer layer of the passive film. These films act as semiconductors or insulators, thus reducing the rate of metal dissolution triggered by an electrochemical potential between a metal and its surrounding electrolyte solution.

The Delhi iron pillar is a 1,600-year old metal artifact (Figure 6-2) that has withstood exposure to the atmosphere with only relatively small amounts of corrosion. Study of the rust layer coating the pillar reveals the presence of crystalline iron hydrogen phosphate hydrate and amorphous iron oxyhydroxides and magnetite (Balasubramaniam 2000 [157383], pp. 2115–2116). The low-porosity crystalline phosphate phase forms a passive film around the pillar, serving to protect it from further corrosion (Figure 6-3). Balasubramaniam (2000 [157383], pp. 2112–2115) interpreted the presence of ~0.25 wt% phosphorous and fine slag particles in the iron to be critical to the development of the corrosion-resistant layer.

6.2.3 Naturally Occurring Metals as Natural Analogues

Josephinite—Josephinite, a naturally occurring Ni-Fe-Co metal-bearing rock consisting of the minerals Ni_3Fe (awaruite), andradite garnet, FeCo (wairuite), and minor to trace amounts of Ni_6Fe_4 and $\text{CaO}\cdot 2\text{FeO}$ (calciowüstite), is a possible natural analogue for Ni-Fe alloys (similar to Alloy 22, which is a Ni-Cr-Mo-W alloy) proposed for the Yucca Mountain waste packages. The

type locality of josephinite is the Josephine Ophiolite, a ~150 million-year-old serpentinized ultramafic body in Oregon, where it occurs within serpentine veins and as coarse metallic nuggets in nearby placer deposits (Dick 1974 [154749]). Josephinite was interpreted by Dick (1974 [154749], p. 297) to be a product of hydrothermal alteration and serpentinization of peridotite. Josephinite and awaruite are very stable rock and mineral phases, as evidenced by their survival for millions of years with only minor amounts of oxidation. Because of this long-lived stability, these ordered Ni-Fe-Co metals (Bassett et al. 1980 [157531]) have been proposed as alloys in constructing containers for the storage of high-level radioactive waste (Bird and Ringwood 1980 [157397]; 1982 [157398]; 1984 [157396]).

Relatively unaltered masses of metal that are predominantly Ni₃Fe (with small inclusions of Ni₃As) were discovered in 1999 within harzburgite in the Josephine Ophiolite and as eroded blocks up to ~3 kg (Bird 2001 [157514]). Preliminary Pb and Os isotopic analyses of these new samples suggest that the josephinite metal did not form as an alteration product of the Josephine Ophiolite, but instead may represent xenoliths within the serpentinite body that have a deep-mantle origin (Bird 2001 [157514]).

The josephinite nuggets have alteration rims comprised of Fe₃O₄ (magnetite, with maghemite) and NiFe₂O₄ (trevorite). Some samples of josephinite contain the high-temperature phase taenite (a disordered Ni-Fe metal) in addition to awaruite (BSC 2001 [155950], Section 7.3.2.4.2). Phase relation studies of the Fe-Ni system suggest that taenite is not stable below ~350°C, and that α-Fe, pure Ni, and awaruite are the stable phases for this system at ambient temperatures (Botto and Morrison 1976 [154716], p. 264). The persistence of taenite for millions of years suggests that low-temperature phase change rates for taenite are exceedingly slow (BSC 2001 [155950], Section 7.3.2.4.2). X-ray photoelectron spectroscopic analysis of a josephinite placer sample from the Josephine Ophiolite (Figure 6-4) revealed that while both iron and nickel are oxidized on the surface, nickel remains in reduced (metallic) form at depths of 2 nm and greater (analyzed to a depth of 120 nm), indicating that the bulk sample has not undergone significant amounts of oxidation (BSC 2001 [157151], Appendix E, Section 3.3.2, Table 1). Because of its high nickel concentrations, the longevity of josephinite indicates that nickel alloys will have long-term phase stability. While josephinite does not contain the molybdenum and tungsten that serve as stabilizing elements in Alloy 22 passive films, its ability to resist corrosion provides confidence that Alloy 22 will remain passive under potential repository conditions (BSC 2001 [157151], Section 3.3.2, Appendix E).

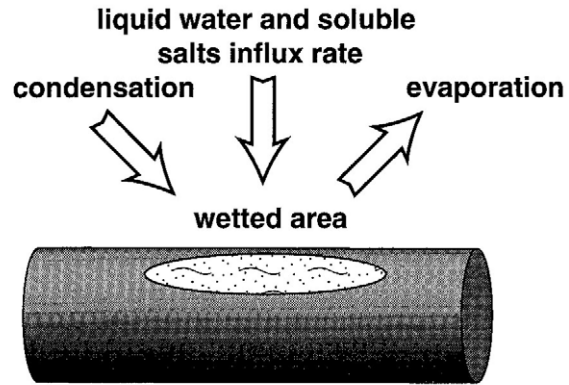
Chromite—Analogues for chromium are considered because of the chromium content of Alloy 22 (Table 5.2). Chromium occurs in minerals in the form of chromite (FeCr₂O₄) and chromium spinel (Mg(Cr,Al)₂O₄). These Cr-bearing minerals are typically found in mafic and ultramafic rocks. Elevated concentrations of chromium in groundwaters in the Leon-Guanajuato valley of central Mexico have been attributed to weathering and alteration of chromite from ultramafic rocks of the Sierra de Guanajuato that have been interpreted to be Jurassic in age (Robles-Camacho and Armienta 2000 [157386], pp. 172–173, 178–181). The San Juan de Otates pyroxenite unit consists of pyroxenite and serpentinized peridotite, harzburgite, and wehrlite. Discrete concentrations of ilmenite and chromite occur within these rocks, and form subrounded masses in outcrop. Chromite is typically found as subrounded crystals, often with exsolution borders of magnetite.

A variety of ultramafic rock samples from the Sierra de Guanajuato, with total chromium contents ranging from 55 to 4115 ppm, were leached with acid to evaluate the susceptibility of the rocks to weathering and subsequent release of chromium (Robles-Camacho and Armienta 2000 [157386], pp. 173–181). The laboratory acid treatment was designed to examine (over a much shorter time scale and under much more acidic conditions than found in the field) the effects of weathering resulting from interaction of oxygenated, CO₂-rich groundwater with chromium-bearing minerals (Robles-Camacho and Armienta 2000 [157386], pp. 174–177). The leachate from Cr-rich serpentinite samples yielded the highest concentrations (up to 274 mg Cr/kg rock), suggesting that they have the greatest potential to release chromium. SEM analysis of samples examined after leaching suggests that dissolution occurred along magnetite exsolution borders of chromite grains (Figure 6-5). Total chromium contents of groundwater samples collected from wells, streams, and reservoirs near the ultramafic rocks range up to 0.0149 mg/L. The Ca-Mg-HCO₃ composition of these waters is consistent with interaction with serpentinized ultramafic rocks. The study does not provide information on the rates of chromite weathering, but it does indicate that chromite exsolution borders are susceptible to chemical attack. This observation is analogous to localized corrosion and pitting observed in metals along structural defects.

6.3 SUMMARY

1. The survival of metal archaeological artifacts over prolonged periods of time is related to the corrosion-resistant properties of metals and metal alloys, the development of protective passive film coatings with the onset of corrosion, and the location of artifacts in arid- to semi-arid environments. Such features can be used in the selection of materials and design configuration to enhance the durability of waste packages at Yucca Mountain.
2. Archaeological examples, such as the Altamira cave, illustrate how environmental changes can significantly affect corrosion behavior. A wide variety of environmental conditions is expected to occur in the near-drift environment at Yucca Mountain during the lifespan of the repository. The introduction of heat-generating waste packages and EBS materials into drifts will perturb the existing physical and chemical system at Yucca Mountain. The materials used for the waste packages (and the rest of the EBS) need to withstand the predicted adverse changes in environmental conditions.
3. Small volumes of concentrated brines could develop in the near-drift environment as a result of evaporation and later dissolution of precipitated salts in the dryout zone with rewetting. High-salinity fluids pose a significant corrosion hazard to carbon steel, as seen at the Salton Sea geothermal field, but the use of titanium alloys can effectively minimize this hazard.
4. The survival for millions of years of the naturally occurring ordered Ni-Fe alloy found in josephinite (with only relatively minor amounts of surface oxidation) indicates that this material is highly resistant to oxidation and other forms of corrosion that occur in its geologic environment. While the composition of this metal differs from Alloy 22 (in that it does not contain Cr, Mo, and W), it does provide evidence that a similar alloy can remain passive over prolonged periods of time.

5. The potential instability of chromium-bearing materials is illustrated by the observed natural release (under ambient conditions) of chromium from chromite in the Sierra de Guanajuato ultramafic rocks. Corrosion appears to be concentrated along exsolution rims, analogous to structural defects on metal surfaces. While the chromite has undergone some alteration, it has survived for over 140 m.y. (since Jurassic time). The corrosion behavior of this chromium oxide mineral may differ from that of the chromium-bearing metal alloys (Section 5) that are currently slated for use in the construction of the waste package.



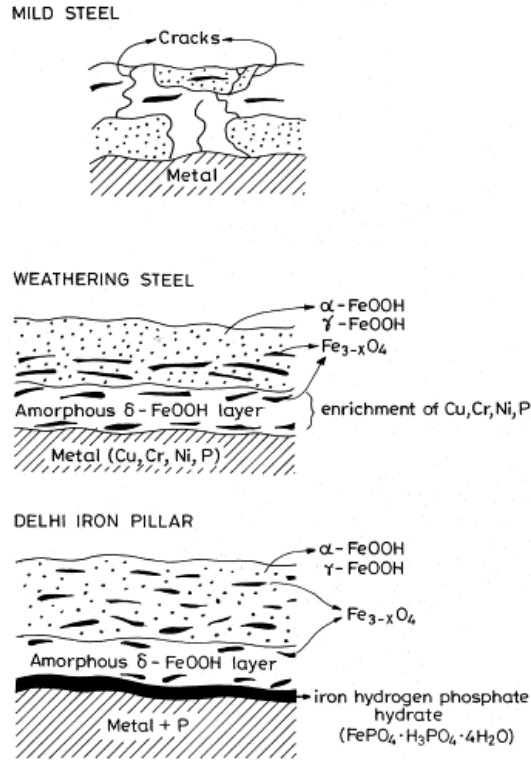
Source: Walton 1994 [127454], Figure 3.

Figure 6-1. Processes Affecting Formation of High-Salinity Fluids on Waste Package Surface



Source: Balasubramaniam 2000 [157383], Figure 1.

Figure 6-2. The Corrosion-Resistant Iron Pillar at Delhi



NOTE: Iron hydrogen phosphate hydrate layer on Delhi iron pillar forms a protective, impermeable coating that retards further corrosion.

Source: Balasubramaniam 2000 [157383], Figure 7.

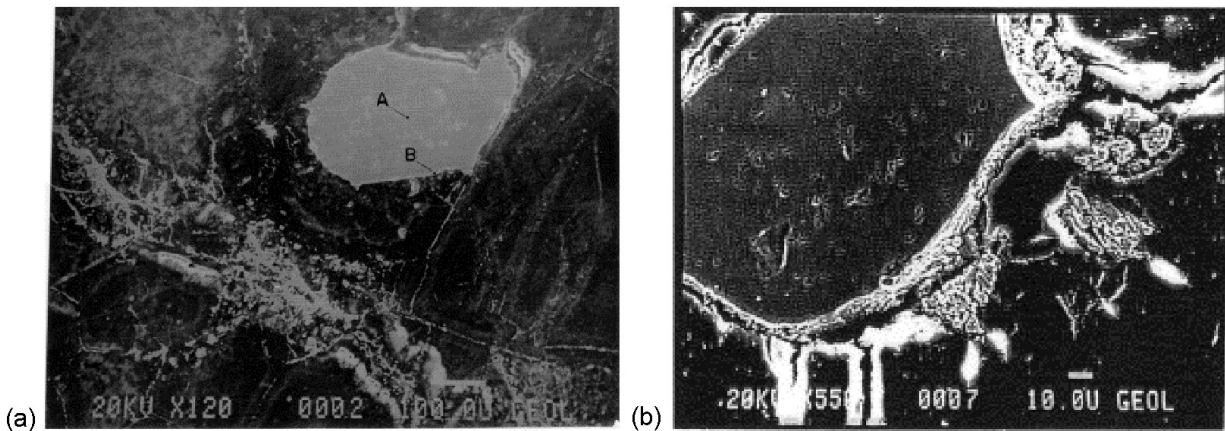
Figure 6-3. Schematic Showing Development of Rust Coating on Mild Steel, Weathering Steel, and Delhi Iron Pillar



NOTE: Metallic-looking areas were analyzed using X-ray photoelectron spectroscopy.

Source: BSC 2001 [157151], Appendix E, Figure 3.

Figure 6-4. Josephinite Sample Used for Surface Analysis Study



NOTE: White rim around chromite in (b) reflects dissolution of exsolution border around chromite.

Source: Robles-Camacho and Armienta 2000 [157386], Figures 5 and 8.

Figure 6-5. Chromite Grains in Serpentinite Before (a) and After (b) Acid Leaching

Table 6-1. Composition of Synthetic Yucca Mountain Waters (mg/L) from Unsaturated and Saturated Zones and Their Evaporated Compositions

	Synthetic J-13 water	"157 x" J-13 water	"956 x" J-13 water	Synthetic UZ water	"62 x" UZ water	"1243 x" UZ water
Na	45.2	5,288	43,302	8.56	477	6,223
K	5.2	593	4,701	4.00	268	2,644
Mg	2.1	1.2	0.13	11.8	550	5,546
Ca	5.8	0.06	27.3	57.3	1,713	15,643
SiO₂	10.4	1,040	----	10.4	503	541
HCO₃	105	4,410	24,255	20.3	9.9	<45
SO₄	18.5	2,109	13,209	83.9	1,544	2,098
Cl	7.2	814	5,047	76.6	4,259	52,165
NO₃	7.9	1,035	5,483	10.7	592	----
F	2.3	237	1,622	2.16	38	<542
TDS	209.6	15,527	97,646	285.7	9,954	~85,000
pH	8.07	10.18	----	7.55	7.65	6–6.5

NOTE: TDS calculated as sum of dissolved solids.

Source: Rosenberg et al. 2001 [154862], Tables 2 and 4.

Table 6-2. Typical Salton Sea Geothermal Well Brine Composition

Component	Concentration ppm	Component	Concentration ppm
Na	49,800	Ba	100
K	12,840	B	301
Mg	80	Cu	7
Ca	24,000	Fe	708
SiO₂	658	Pb	66
CO₂	125	Li	177
SO₄	22	Mn	785
Cl	126,700	Rb	62
NH₃	339	Sn	402
As	8	Zn	287
I	5	Br	68
pH	5.8	H₂S	90
		TDS	261,800

Source: Pye et al. 1989 [157385], Table 1.

7. ENGINEERED BARRIER SYSTEM ANALOGUES

7.1 INTRODUCTION

This section describes the use of natural analogues to evaluate the long-term performance of materials used in the construction of the Engineered Barrier System (EBS) and how these materials may affect radionuclide transport. The primary functions of the EBS components are to: (1) protect the waste package from physical and chemical degradation resulting from processes such as seepage, corrosive fluids, and rock fall; and (2) retard any potential transport of radionuclides from the emplacement drift in the event of waste package failure. Key concerns for the EBS materials (described in Section 5) include the possible degradation and corrosion of metals resulting from mechanical stress, hostile physical and chemical environments, and metallurgical factors. Another important performance parameter is the effect of EBS materials on flow and transport of fluids and dissolved solids into and out of the emplacement drifts. Important issues relating to EBS performance include the degradation of materials caused by corrosive fluids, radiation, thermal and physical stresses, and microbial attack, as well as the effects of sorption and colloids on radionuclide transport. A number of analogues were previously discussed in Section 13 of the *Yucca Mountain Site Description* (CRWMS M&O 2000 [151945]); these analogues are briefly summarized below. Additional analogue examples are discussed in more detail in the following subsections.

Three main issues relating to the EBS were discussed in detail in the natural analogues chapter of the *Yucca Mountain Site Description* (CRWMS M&O 2000 [151945], Section 13.3): (1) metal analogues (native metals and archaeological artifacts) in the evaluation of corrosion resistance; (2) cements and alkaline plumes to determine the impact of high pH fluids on EBS materials, surrounding host rock, and radionuclide transport; and (3) the effects of radiolysis on the integrity of waste package materials. A brief summary of earlier work on metal analogues is presented in Section 6 and thus will not be repeated here.

Under the current EBS design, cementitious material is expected to be present in only minor amounts (as grout for rock bolts) in the near-drift environment. The durability of cements over time has been documented by Gallo-Roman cements that are over 1,500 years old (Thomassin and Rassineux 1992 [157439], p. 137). Cementitious mortar from Hadrian's Wall (~1,700 years old) in England (Figure 7-1) has the same calcium silicate hydrate phases found in modern Portland cement, and still possesses excellent strength and stability (Miller et al. 2000 [156684], p. 131). The potential development of hyperalkaline fluids resulting from interaction of water with cementitious material could affect radionuclide transport and reduce the stability of EBS materials. Two areas with hyperalkaline fluids were described in the earlier review of natural analogues (CRWMS M&O 2000 [151945], Section 13.3.6): the Semail ophiolite in Oman, and the Maqarin area in Jordan. Serpentinization reactions in the Semail ultramafic rocks have resulted in the generation of reducing, hyperalkaline (pH = 10–12) Na-Cl-Ca-OH fluids, with associated minerals brucite ($\text{Mg}(\text{OH})_2$) and portlandite ($\text{Ca}(\text{OH})_2$). The Maqarin analogue site (also discussed in Section 7.3.1) contains a suite of naturally formed cement minerals, including portlandite. High pH (12–13) fluids emanate from these rocks as a result of reaction of groundwater with the cement phases. These analogue sites have been used in the development of

numerical models to predict water-rock reactions and resulting fluid compositions under similar conditions (McKinley et al. 1988 [126077]; Chambers et al. 1998 [157549]).

Chemical decomposition resulting from radiation (radiolysis) was also examined in the *Yucca Mountain Site Description* (CRWMS M&O 2000 [151945], Section 13.3.7). This process was studied at the natural reactor site at Oklo (in Gabon), where high radiation doses were interpreted to have led to radiolysis of water and redox reactions involving the surrounding rocks (Curtis and Gancarz 1983 [124785]). Similar reactions within the waste package assembly could lead to decomposition of the waste packages and release of radionuclides. However, since the waste loads are configured so that they will not approach criticality and the waste package design excludes free water, the amount of radiolysis that might occur at the potential Yucca Mountain repository should be much less than Oklo (see also Section 4 of this report). Section 7.2 describes analogues for EBS materials and Section 7.3 describes analogues for EBS processes.

7.2 ANALOGUES FOR EBS MATERIALS

7.2.1 Analogues for the Titanium Drip Shield

Corrosion caused by saline fluids has been identified as a potential hazard to the integrity of waste packages (see Section 6.2.1 for discussion). The drip shield assembly is designed to protect the waste packages from physical and chemical degradation resulting from events such as rock falls, seepage, and saline fluids. The current drip shield design calls for corrosion-resistant titanium. Titanium metal does not occur in nature, nor in the archaeological record, so other proxies need to be used to assess its long-term resistance to corrosion.

The Salton Sea geothermal field in California is characterized by hypersaline (15-30 wt% TDS) brines that have caused significant corrosion and scaling problems (Pye et al. 1989 [157385], p. 259). A series of corrosion tests led field operators to select Beta-C titanium (Ti-3Al-8V-6Cr-4Mo-4Zr) for the fabrication of corrosion-resistant production casing (Pye et al. 1989 [157385]). Four tests were conducted over a period from 256 to 833 days, involving installation of full-size Beta-C titanium tubulars in geothermal production wells, resulting in no visible pitting corrosion in two of the tests, little or no change in hydrogen content, and no significant degradation in mechanical properties (Pye et al. 1989 [157385], pp. 262–263). In the 833-day test, localized corrosion was observed, occurring at a rate of 7 mils/yr (178 $\mu\text{m}/\text{yr}$); this was interpreted to have occurred in an area where surface contamination had not been completely removed at the start of the test. Local corrosion was observed along 2 of the 48 casing joints in the fourth test; this corrosion was also interpreted to be the result of pre-existing surface contamination.

A longer-term evaluation of the corrosion behavior of titanium-bearing materials can be obtained by examining the stability of naturally occurring titanium minerals. Titanium is present as a major constituent in a number of refractory accessory minerals commonly found as a minor phase in igneous rocks and in heavy mineral concentrates in sediments. These minerals include sphene (titanite) ($\text{CaTiSiO}_4(\text{O},\text{OH},\text{F})$), rutile (TiO_2), ulvöspinel (Fe_2TiO_4) and ilmenite (FeTiO_3). The Canadian nuclear waste disposal concept includes a metallic titanium container surrounding spent fuel. The corrosion resistance of titanium arises from its passivation in aqueous solutions

by the formation of a protective layer containing rutile (Cramer 1994 [157537], pp. 8–10). At the Cigar Lake uranium deposit in Saskatchewan, Canada, rutile is present within the uranium ore and has persisted unchanged for over a billion years in reducing groundwaters, under hydrothermal conditions, and in a radiation field. While rutile and other titanium-bearing minerals are oxides, and thus do not share the same physical properties as metals, their general resistance to alteration reflects the stable nature of titanium-bearing materials.

7.2.2 Analogues for the Invert Ballast

The nonwelded Calico Hills Formation and portions of the Paintbrush Tuff at Yucca Mountain are possible analogues for processes, such as sorption and ion exchange, that would affect the transport of radionuclides within the crushed tuff invert ballast. The relative lack of fractures in these tuffs results in fluid flow occurring in the tuff matrix, resulting in overall slower fluid flow and transport in these units caused by the lack of fast flow pathways, similar to what is predicted for the crushed tuff invert. Because of the presence of zeolites and/or smectite in the nonwelded tuffs, extensive ion exchange occurs between pore waters and the tuffs (Vaniman et al. 2001 [157427]). The zeolitic tuffs are significantly enriched in cations such as Ca^{2+} , Mg^{2+} , and Sr^{2+} , and depleted in Na^+ and K^+ (Figure 7-2); thus, waters are interpreted to have complementary (opposite) enrichments and depletions (Vaniman et al. 2001 [157427], pp. 3420–3423). This ion-exchange process would have a major impact on radionuclide transport, with species such as ^{90}Sr being effectively immobilized by this process. However, the current design for the invert ballast (DOE 2001 [153849], Section 2.4.1.2) uses crushed tuff derived from the repository interval (welded, devitrified Topopah Spring Tuff), which has only minor amounts of zeolites and clays (Vaniman et al. 2001 [157427], Figure 2). As a result, the ion exchange and sorption capacity of the crushed tuff invert ballast should be significantly lower than that observed in the nonwelded tuffs at Yucca Mountain. The crushed tuff invert would have high effective grain surface areas, which would favor sorption of species onto mineral surfaces, thus serving to retard radionuclide transport.

The effects of fluid flow on radionuclide retardation in ash flow tuff can also be evaluated through an anthropogenic analogue. At Los Alamos National Laboratory, radionuclide-bearing liquid wastes were discharged from 1945 to 1967 into gravel- and cobble-filled absorption beds (approximately 6 m × 37 m) built on outcrops of moderately welded rhyolite ash flow tuff (Figure 7-3) (Nyhan et al. 1985 [157447], p. 502). Large amounts (corresponding to a depth of 20.5 m) of tap water and radioactive effluent were added to one of the absorption beds (Bed 1) in 1961 to evaluate radionuclide mobility. The site was revisited in 1978, when profiles of Pu and ^{241}Am were measured in a series of 30.5 m deep boreholes drilled through two of the absorption beds (Bed 1 and Bed 2) and into the underlying ash flow tuff (Nyhan et al. 1985 [157447], p. 502). This study revealed that the bed where water and effluent had been added in 1961 (Bed 1) exhibited higher water saturations, along with significantly more radionuclide migration out of the absorption bed and into the underlying tuff (Figure 7-4), than the bed where no additional fluid had been added during this test (Bed 2). Plutonium and ^{241}Am were not detected beyond 11.28 m below the bottom of Bed 2, whereas 0.3 to 5.1% of the plutonium and 3.0 to 49% of the americium inventory were present within the depth interval of 11.28–27.13 m for Bed 1 (Nyhan et al. 1985 [157447]), p. 506). Elevated concentrations of radionuclides were observed to occur within lower permeability intervals of the tuff. The radionuclide concentrations of fracture fillings were similar to those of adjacent tuff samples, suggesting that fractures did not enhance

radionuclide transport under unsaturated conditions and generally acted as barriers to unsaturated zone (UZ) flow (Nyhan et al. 1985 [157447], pp. 504–505, 508). These results suggest that radionuclide mobility was triggered by flushing of the absorption beds with large volumes of fluids. The volume of the column of fluid used in the Los Alamos test is equivalent to the amount of percolating surface water expected to flow through Yucca Mountain over a timespan of 2,000 to 4,000 years (assuming an infiltration rate of 5 to 10 mm/yr (Flint et al. 2001 [156351], p. 26), and thus represents an illustration of the effects of flushing on radionuclide mobility. However, this example does suggest that the ability of the invert ballast at Yucca Mountain (as well as the underlying welded tuffs) to retard radionuclide migration will depend in part on the amount of water flowing through this interval. Both of the analogue examples described are also relevant to processes controlling radionuclide transport in the UZ at Yucca Mountain (see Section 9).

7.3 NATURAL ANALOGUES FOR EBS PROCESSES

The physical and chemical conditions for the near-field area around the emplacement drifts at Yucca Mountain are predicted to undergo changes over time. These changes would result from coupled thermal-hydrologic-chemical (THC) processes, such as boiling, condensation, fluid flow and transport, and mineral dissolution, alteration, and precipitation (BSC 2001 [154677]). THC processes are also expected to occur within the EBS, and could lead to degradation of the EBS components, resulting in the release and transport of radionuclides away from the EBS. Natural analogue studies for some of the processes expected to impact the EBS system, such as the generation of alkaline plumes resulting from interaction of water with cementitious material and the effects of colloids on radionuclide transport, are described below.

7.3.1 Natural Analogues for Development of Alkaline Plumes from Cement

The presence of naturally occurring cement minerals and associated hyperalkaline groundwaters at Maqarin, Jordan, has been used as a natural analogue for examining the effects of hyperalkaline waters (e.g., Khoury et al. 1992 [125677]; Smellie 1998 [126633]). The Maqarin site consists of interbedded bituminous limestones and marls that have been locally thermally metamorphosed from spontaneous combustion of the bitumen, resulting in the calcination of limestone and formation of cement minerals, including portlandite. Water interacting with portlandite has resulted in the formation of highly alkaline (pH \approx 12.5) groundwaters and the precipitation of minerals such as ettringite and thaumasite at ambient temperatures (Figure 7-5). Initial geochemical modeling efforts resulted in model predictions of dissolved selenium and uranium concentrations that were several orders of magnitude higher than those observed in the field (Linklater et al. 1996 [108896], p. 67). A multicomponent reactive transport model that incorporated mixed equilibrium and kinetic reactions was applied to simulate rock alteration mineralogy and fluid chemistry changes for discrete fractures in the Maqarin system (Steeffel and Lichtner 1998 [156714]). These simulations predict the formation of hydrated calcium sulfate and silicate minerals, such as ettringite and tobermorite, which were observed in the field (Khoury et al. 1992 [125677], p. 122), and also reproduced measured fluid pH values. The simulations suggest that mineralization caused by interaction of the hyperalkaline plume with surrounding rocks may result in both reduction of matrix porosity and fracture sealing. Fractures at the Maqarin site have complex mineralogy and textures that suggest that they have undergone repeated sealing and reopening over time. The relative rates of matrix and fracture mineralization

(and associated reduction in permeability) will significantly affect the mobility of the alkaline plume, and thus the transport of associated radionuclides.

The development of large hyperalkaline plumes and associated alteration and transport are not expected to occur at Yucca Mountain. The amount of cementitious material expected to be present in the potential repository (in the form of grout around rock bolts in the emplacement drifts) is much less than what is observed at Maqarin. The fluid pH of the near-field environment thus will be buffered by tuff rather than by portlandite, resulting in less alkaline pH conditions (DOE 2001 [153849], Section 4.2.3.3.3). The Maqarin natural analogue is important to consider in illustrating the effects of alkaline fluids on water-rock processes, and thus constraining EBS design parameters (through minimization of the use of cement) and coupled process models. The ability of the multicomponent reactive transport simulations to reproduce observed water-rock interactions for the alkaline plumes at Maqarin provides confidence that similar THC modeling efforts at Yucca Mountain predict reactive chemistry and transport processes that are expected to occur over time.

7.3.2 Natural Analogues for Colloidal Transport of Radionuclides

Colloids can facilitate radionuclide transport (Figure 7-6) if they are: (1) present in sufficient quantities, (2) mobile, and (3) can bind radionuclides (Wieland and Spieler 2001 [157442], p. 511). Naturally occurring colloids are ubiquitous in groundwaters; sampled by Kingston and Whitbeck (1991 [113930], pp. 26, 57) (mainly from central and southern Nevada) have dilute colloid concentrations ranging from 0.28–1.35 mg/L), and ferric oxide and oxyhydroxide colloids can also be generated through degradation of structural steel present in EBS materials.

Filtration of Fe-bearing colloids has been documented in some environments. For instance, groundwaters in the Poços de Caldas area, Brazil, typically have low concentrations (<1 mg/L) of colloids (Miekeley et al. 1989 [126083], pp. 838, 840–841; 1991 [127199], pp. 35, 49). Most of the colloids there are composed of iron and organic species. Only minor amounts of uranium are associated with colloids, but greater amounts of thorium and rare earth elements are transported in the colloidal fraction. The results of the colloid studies at Poços de Caldas (Miekeley et al. 1989 [126083], p. 841; 1991 [127199], p. 58) suggest that radionuclide and other trace-element transport by colloids does not play a significant role in the geochemical processes of weathering, dissolution, and erosion of these ore deposits. One reason for this could be filtration of material which traps colloids in pore throats and narrow fractures (Smellie et al. 1989 [126636], p. 868). The colloidal material acts as an efficient and largely irreversible sink or trap for many elements (especially if they are immobile), but needs to be taken into account in equilibrium thermodynamic modeling of radionuclide speciation. The point of this example is that the iron-bearing colloids that may form in the Exploratory Studies Facility could be beneficial in complexing with uranium and could be retained effectively in the EBS by filtration.

7.4 SUMMARY

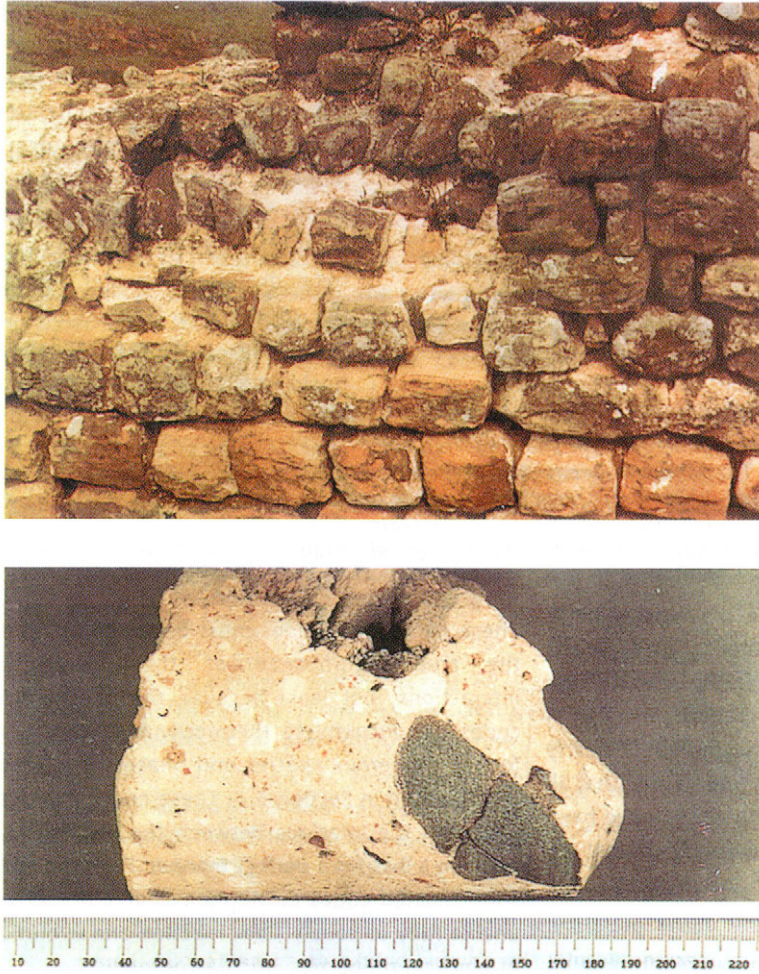
The highly corrosive-resistant nature of titanium has been demonstrated by long-term experiments conducted on a range of metal alloys in wells at the Salton Sea geothermal field. The commercial use of titanium alloys in production casings over the past decade at the Salton Sea has greatly alleviated severe corrosion problems that were previously experienced resulting

from exposure of conventional steel casing to the hot, hypersaline geothermal brines. This anthropogenic example supports the selection of titanium alloys for the construction of a corrosion-resistant drip shield for the EBS.

Mineralogic and geochemical analysis of tuffs in the UZ at Yucca Mountain indicates that the presence of zeolite and clay minerals greatly enhance cation exchange, thus serving to retard the transport of some radionuclides. While the proposed material (devitrified welded tuff) for the invert ballast in the current design does not have high concentrations of these minerals, the high surface area of crushed tuff will retard radionuclide transport through absorption. The Los Alamos example of actinide absorption in a gravel bed provides qualitative evidence of retardation at the contact between an invert-like material and underlying bedrock.

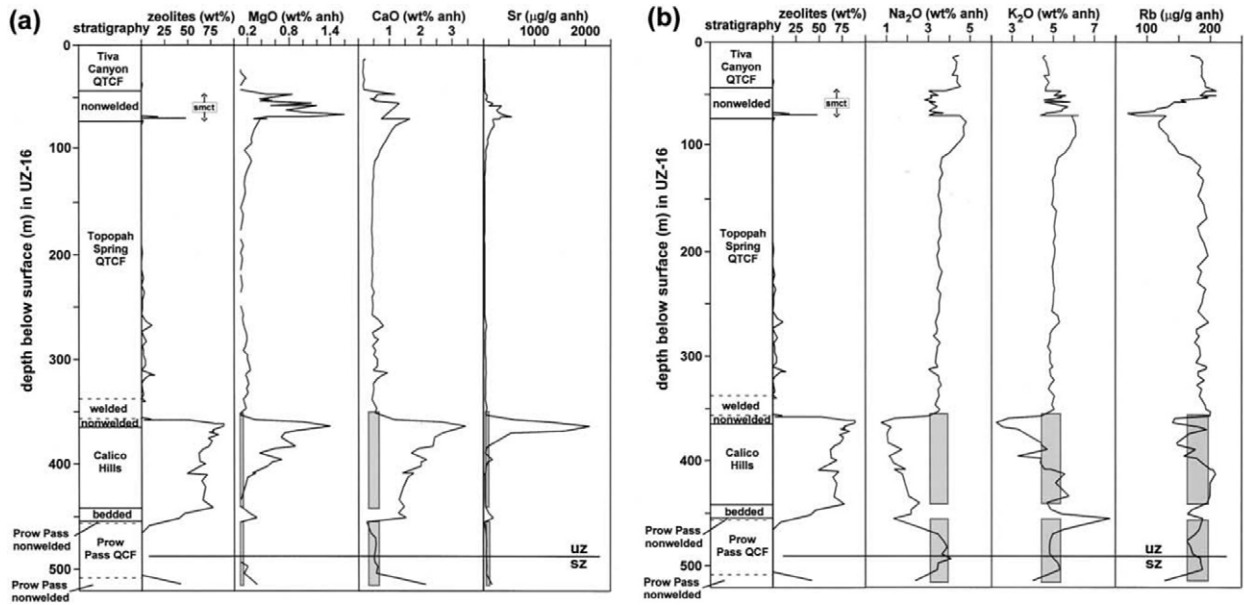
The presence of cementitious materials can potentially lead to the development of alkaline plumes, resulting in corrosion of waste package materials, alteration of surrounding host rocks, and possible enhancement of radionuclide transport. Because the use of cementitious material in the EBS and its environs is restricted to grout for securing rock bolts in the emplacement drifts, hyperalkaline conditions are not expected to develop at Yucca Mountain. However, through reactive transport modeling of the Maqarin site, it has been demonstrated that a model can reproduce the same suite of cement minerals, hyperalkaline water compositions, and pH that were found in the field, thus building confidence in use of such a model for analogous conditions at other sites.

The Poços de Caldas analogue illustrated that iron-bearing colloids may retard the transport of uranium and other spent-fuel components by forming colloids that are then filtrated from suspension at short distances. Degradation of steel structural elements in the EBS could conceivably contribute to this process.



Source: Miller et al. 2000 [156684], Figure B10.2.

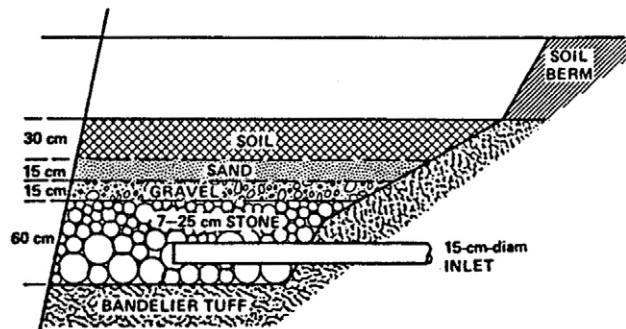
Figure 7-1. Portion of Hadrian's Wall in England, Showing Strength and Stability of Roman Mortar after 1,700 Years



NOTE: Shaded bars represent corresponding compositions of unzeolitized precursor tuffs. Symbols (Q = quartz, T = tridymite, C = cristobalite, F = feldspar) indicate devitrification minerals in welded tuff intervals. UZ-SZ line marks location of water table. Chemical abundances are normalized to anhydrous (anh) compositions.

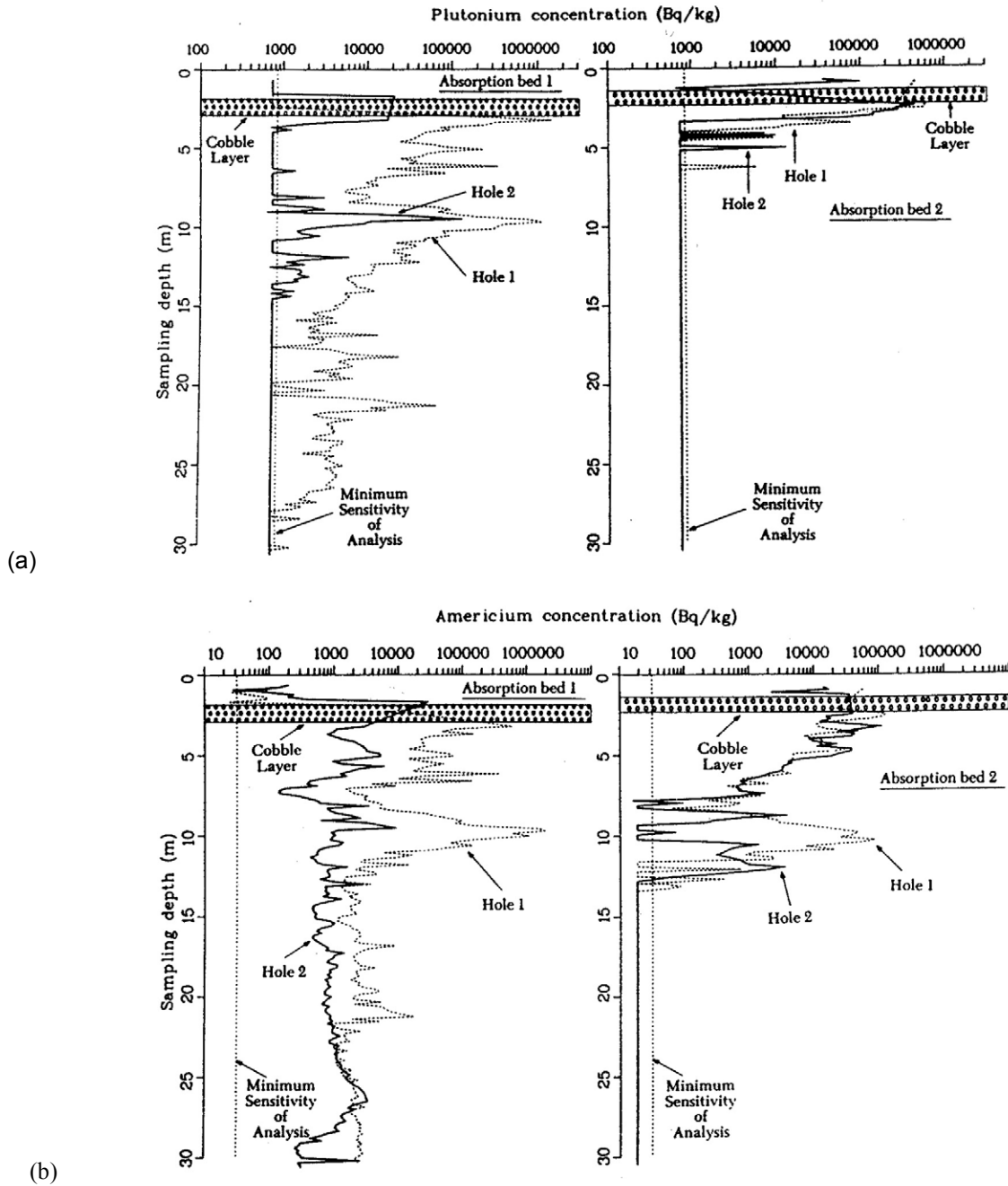
Source: Vaniman et al. 2000 [157427], Figure 4.

Figure 7-2. Stratigraphic Section of Drill Hole UE-25 UZ#16, with Abundance of Zeolites Plotted versus (a) Alkaline Earth and (b) Alkali Constituents



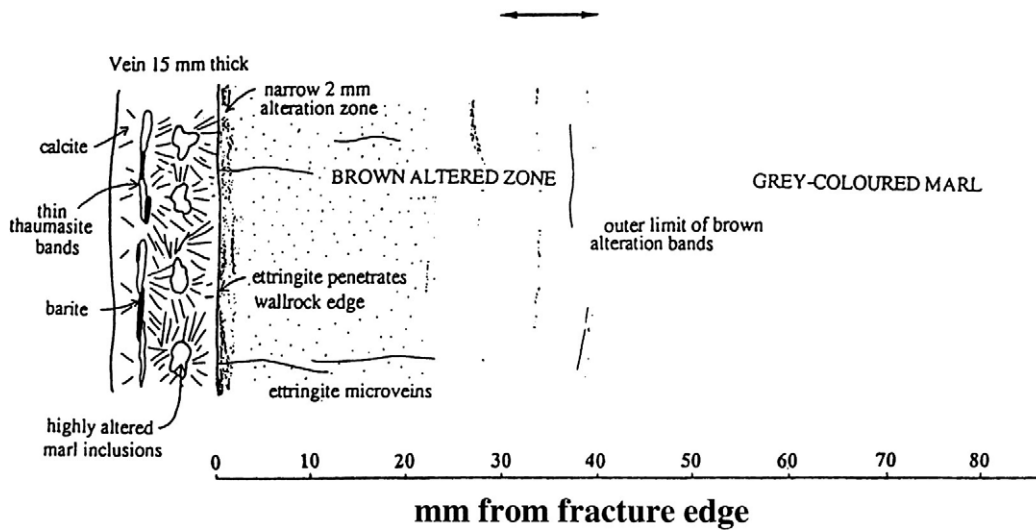
Source: Nyhan et al. 1985 [157447], Figure 1.

Figure 7-3. Cross Section of Absorption Bed for Disposal of Radioactive Liquid Wastes, Area T, DP West Site, Los Alamos National Laboratory



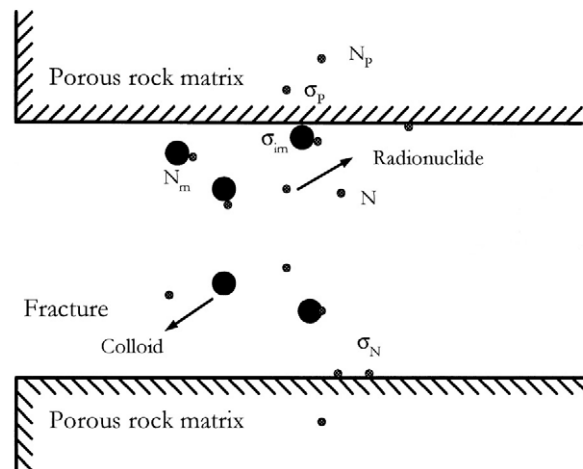
Source: Nyhan et al. 1985 [157447], Figures 2 and 3.

Figure 7-4. Concentrations of Plutonium (a) and Americium-241 (b) within and beneath Absorption Beds 1 and 2, Area T, DP West Site, Los Alamos National Laboratory (1978)



Source: Steefel and Lichtner 1998 [156714], Figure 6.

Figure 7-5. Fracture Mineralization and Wall Rock Alteration at C353 Site, Maqarin, Showing the Presence of Hydrated Calcium Silicate and Sulfate Phases Thaumasite and Ettringite



NOTE: N = dissolved radionuclides in fracture,
 σ_N = radionuclides on fracture surface,
 N_m = radionuclides bound to mobile colloids,
 σ_{im} = radionuclides sorbed on immobile colloids,
 N_p = dissolved radionuclides in pores of rock matrix,
 σ_p = radionuclides sorbed on rock matrix.

Source: modified from Jen and Li 2001 [157463], Figure 1.

Figure 7-6. Schematic Illustration of Radionuclide Transport in a Fractured Rock

8. NATURAL ANALOGUES FOR SEEPAGE

8.1 INTRODUCTION

This section examines several different types of qualitative and quantitative natural analogues for seepage, taken from caves, lava tubes, tombs, rock shelters, and buildings that were investigated since publication of the *FY 01 Supplemental Science and Performance Analyses* [SSPA], *Volume 1: Scientific Bases and Analyses* (BSC 2001 [155950]). It considers the role of the hydrogeologic setting of underground openings on seepage and the effect of relative humidity. It evaluates a number of candidate settings that have been suggested as analogues and demonstrates why they are or are not considered appropriate as seepage analogues. It also examines the question of the preponderance of evidence of preservation of seepage analogues. In this section, the term *infiltration* is used for precipitation that is not lost by runoff, evaporation, or transpiration, and *seepage* is used for that portion of the infiltration within the unsaturated zone (UZ) that enters tunnels or other underground openings. For reference, current precipitation at Yucca Mountain is about 190 mm/yr (DOE 2001 [153849], Section 4.2.1.2.1), with future rates predicted to be 269 to 529 mm/yr (BSC [155950], Table 3.3.1-5). Information found in Sections 8.2, 8.3, and 8.4 may help to support arguments associated with Key Technical Issue (KTI) KUZ0407 found in Table 1-1.

8.2 GEOLOGIC EXAMPLES

Seepage is mainly governed by the capability of individual fractures to hold water by capillary forces, and by the permeability and connectivity of the fracture network, which enables water to be diverted around a drift or underground opening. Both properties determine the effectiveness of the capillary barrier in diverting flow and thus reducing seepage rates below the prevailing percolation flux. Percolation is the downward or lateral flow of water that becomes net infiltration in the UZ. The physical properties of water, together with the hydrologic properties of rock, lead to the prediction that much of the infiltrating water in the UZ will be preferentially diverted around openings, such as tunnels, at the potential mined geologic repository at Yucca Mountain. The percentage of infiltration that can become seepage decreases as infiltration decreases, and at low infiltration rates (<5 mm/yr) and most permeabilities, no seepage occurs (DOE 2001 [153849], Section 4.2.1.4.2). Two natural analogue studies confirm the prediction that most infiltration does not become seepage.

In a two-year study at Kartchner Caverns, Arizona, yearly precipitation ranged from 288 mm to 607 mm, and averaged 448 mm/yr (Buecher 1999 [154295], pp. 108–109). This was similar to the long-term average at two nearby stations. Estimates of seepage into the cave by three methods based on infiltration and precipitation measurements ranged from 4.3 mm/yr to 12.4 mm/yr, with an average of 7.9 mm/yr (Buecher 1999 [154295], p. 110). Thus, less than 2% of the available moisture became seepage. This low seepage occurs even though the cave, which covers an area of approximately 350 m (N-S) by 550 m (E-W), is cut by more than 60 mapped faults (Jagnow 1999 [154296], p. 49 and Figure 3).

The cave at Altamira, Spain, was monitored for 22 months by Villar et al. (1985 [145806]). The volume of water flowing from 9 of 14 “significant drips” was measured, and an average total

seepage of 7 liters/mo was reported. This volume is estimated to represent about 80% of the total seepage (Stuckless 2000 [151957], p. 6), which would bring the total seepage rate up to almost 9 liters/mo. Villar et al. (1985 [145806], Figure 4) also measured the average rainfall. Based on the data from Villar et al. (1985 [145806], Figure 4) the average annual rainfall was calculated to be approximately 1152 mm/yr or 1152 liters/yr/m² (Simmons 2002 [157544], p. 144). The average evapotranspiration was calculated as approximately 660 mm/yr (660 liters/yr/m²), which results in an average net infiltration of about 480 mm/yr (480 liters/yr/m²). The area of the painted cave studied was reported as 150 m², which would result in a monthly volume of infiltration water of about 6,000 liters/mo above the footprint of the area studied in the cave (Simmons 2002 [157544], pp. 143–144). As was the case at Kartchner Caverns, the rock is obviously fractured (Figure 8-1). Nonetheless, less than 1% of the infiltrating water seeped into the cave. The fact that the paintings have not been bleached or dissolved near the fractures suggests that little water has seeped in along fractures during the last 14,000 yrs, which is the age of the paintings (Stuckless 2000 [151957], p. 8).

Both of these examples are from limestone caves in fractured karst terrain. It follows from these examples that UZ flow would be dominated by fracture flow, just as it is at Yucca Mountain. Both caves are much closer to the surface than a potential repository at Yucca Mountain, and therefore, there is a much greater probability for fractures to communicate directly between the underground opening and the surface, thereby facilitating seepage. At the caves, a pulse of water enters at peak saturation, whereas at the potential repository horizon the amplitude of the water pulse is attenuated because of the damping effect of the PTn (BSC 2001 [155950], Section 3.3.3.1). This damping effect yields lower average saturations that are less conducive to seepage. At both Altamira and Kartchner Caverns, precipitation exceeds current rates at Yucca Mountain and those predicted for future climates as well. Thus, the observational data from these natural analogues support the conclusion that seepage into a potential repository at Yucca Mountain would be a very small percentage of the percolation flux, which will therefore result in a very small volume of water entering drifts.

8.3 ARCHEOLOGICAL EXAMPLES

The long-term quantitative hydrologic studies such as those cited above are not common, but there is abundant qualitative evidence that openings in the UZ divert much infiltration, thereby protecting fragile and easily destroyed items. The examples that follow are from both natural and man-made underground openings and include preservation of both anthropogenic and biological materials. The examples chosen are representative and are not meant to constitute an exhaustive listing.

The oldest and perhaps the best known examples of preservation of anthropogenic items within the UZ are the Paleolithic cave paintings of southwestern Europe. The Paleolithic cultural period lasted from 750,000 to 15,000 years ago. There are dozens of caves with paintings (Stuckless 2000 [151957], Figure 1); the oldest of those authenticated is the recently discovered cave of Chauvet, France (Figure 8-2). The cave is located in a subhumid region, with reported precipitation totals within the region ranging from 580 to 780 mm/yr (Stuckless 2000 [151957], p. 3). The Chauvet cave paintings depict animals that are now extinct, such as mammoths, and other species that no longer live in Europe, such as rhinoceroses (Chauvet et al. 1996 [152249]), which attest to a much different paleoclimate from the climate at present. The paintings in the

French caves were made largely with oxides of iron and other minor constituents (Leroi-Gourhan 1982 [156454] p. 105; Ruspoli 1987 [156223], pp. 192–193). Charcoal or manganese oxide was commonly used for black. Neither the iron and manganese oxide nor charcoal would be expected to survive long in the presence of abundant oxidizing water. This is evidenced by a painted block that fell from a painting of a bull at Lascaux, France, and lay painted side down on the damp floor. Although the block fit back into the painting, it had lost all evidence of paint (Breisch 1987 [156456], p. 286).

Well-preserved Paleolithic art is common only in the caves of southern Europe, but examples of late Paleolithic and, more commonly, Neolithic art from the Neolithic cultural period that began about 10,000 B.C. are known throughout the world. Stuckless (2000 [151957]) provides a summary and references for paintings in Africa, South America, North America, and Asia. In most of the world, painted rock shelters are more common than painted caves, which demonstrates that even a few meters of overhang can protect fragile art from infiltration water (Stuckless 2000 [151957], p. 9).

In addition to paintings, caves have preserved fragile artifacts such as the 14,000-year-old clay bison in a cave near Tuc d'Audoubert, France (Stuckless 2000 [151957], Figure 3). Some caves are located in zones of such low percolation flux that they have little, if any, measurable seepage flux. This supports another part of the UZ flow model in which seepage is predicted to decrease with a decrease in infiltration. Caves in Israel provide an example of this, where cloth, ivory, reed mats, and many bronze items have been preserved in a nearly perfect state (Schick 1998 [156641], Color Plates 3.7–3.9; Ozment 1999 [155058], pp. 74–75). These date from about 3,800 B.C., and although the climate is currently drier than that at Yucca Mountain, the preservation demonstrates that the lack of water allows even easily destroyed items to endure for long periods of time and suggests that the predicted zero seepage at low infiltration rates is likely correct.

Relatively dry caves are common throughout the southwestern United States. Because of the dryness, pollen and other delicate plant and animal materials have been preserved for tens of thousands to hundreds of thousands of years (Davis 1990 [144461]; Rogers et al. 2000 [154320]) in caves and lava tubes, respectively. In fact, Davis (1990 [144461], p. 338) notes that dryness in caves is critical to preservation of biotic remains. That such preservation is common is supported by the fact that over 1,000 packrat middens have been studied throughout semi-arid to arid North America, and some of these are older than 40,000 yrs (Davis 1990 [144461], p. 341). The middens are cemented with dried urine, which would dissolve readily in water. Nonetheless, the middens older than about 20,000 yrs (some of these were found near Yucca Mountain) have survived much wetter past climates, similar to those predicted for the future climate at Yucca Mountain, indicating that over a long period of time, little seepage has entered the openings where middens were found.

Underground openings in the UZ have been excavated by early civilizations, but these examples are generally much younger than those from natural systems. Nevertheless, they also provide evidence of the robust protection provided against the effects of water. In addition, these anthropogenic examples broaden the range of geologic settings that can be examined as analogues for a potential repository at Yucca Mountain.

Man-made underground openings include the Egyptian tombs across the Nile River from Luxor. These were excavated in limestone approximately 3,500 to 3,000 years ago. As noted in Section 8.2, this host rock is hydrologically similar in fracturing and low matrix porosity to the welded tuffs of Yucca Mountain. Although the climate is somewhat drier than that at Yucca Mountain, precipitation events have been strong enough to cause mud flows within the Valley of the Kings (Weeks 1998 [154297], pp. 10, 11). Seepage into the tombs is indicated by small areas of spallation of plaster, which can be seen in many tombs for both areas of wall and ceilings (Figure 8-3), but evidence of dripping, such as efflorescence or stalactitic formations, seems to be lacking.

Buddhist monks carved several temples into basalt flows at Ajanta, India, between the second century B.C. and the tenth century A.D. (Behl 1998 [156213], p. 27, 39). Water flow within the basalts would, as at Yucca Mountain, be dominated by fracture flow. The interiors of the temples are painted. The paintings were done on a plaster that consisted of mud, rock dust, and vegetable fiber. The climate at Ajanta is monsoonal, such that the precipitation (800 mm/yr), which is more than four times that at Yucca Mountain (Section 8.1), falls in four months (Stuckless 2000 [151957], p. 19). Nonetheless, many of the paintings are well preserved, except for small areas of spallation (Figure 8-4).

The Christians of Cappadocia, Turkey, excavated underground cities and churches during the second through eleventh centuries A.D. The geology here is similar to that of southern Nevada in that the bedrock is a thick sequence of silicic volcanic rocks. Visits to the underground cities and churches produced no evidence of dripping from the ceiling, but evidence for flow down a wall was found where a fracture intersected the wall (Stuckless 2000 [151957], p. 22). As with the Egyptian tombs and Buddhist temples, some of the church paintings showed evidence of spallation (Figure 8-5).

The caves at Carlsbad Caverns, New Mexico have stood open for as much as 11 m.y. (Polyak et al. 1998 [156159], p. 1919). During that time, seepage occurred as evidenced by stalactites, stalagmites, and flowstone. Today, only a small percentage of the seeps are active in spite of an average precipitation of approximately 500 mm/yr. This is more than twice the amount currently observed at Yucca Mountain and larger than that predicted for likely future climates.

In addition to showing that most infiltration does not become seepage, natural analogues demonstrate that much of the seepage that does occur stays on the walls rather than dripping into the openings. Figures 8-2 and 8-3 show evidence of water flow down walls. Figure 8-6 shows the soot-covered wall and ceiling of a kitchen excavated in the tuffs of Goreme (Cappadocia region), Turkey. The soot deposited along the fracture in the ceiling has been bleached out, presumably because of infiltrating oxygenated water. Stalagmitic deposits that might indicate dripping water do not exist, but the removal of soot below the fracture on the wall would have to be caused by some flow of water down the wall.

Perhaps the best analogue for water that might seep into the tunnels at Yucca Mountain can be seen at Building 810 in the Denver Federal Center, Colorado (Figure 8-7a). The roof of this building is constructed of a series of arches called barrels. Each represents a segment of a cylinder with a diameter of 25 ft, the same diameter as the Exploratory Studies Facility (ESF) at Yucca Mountain. As shown by the white efflorescent salt deposits, water has seeped through the

roof over the loading dock along fractures in the concrete and then flowed on the underside of the roof, until it either evaporates or reaches the vertical sections along the sides of the barrels, where it can drip. The undersurface shown in Figure 8-7b is smoother than much of the ESF tunnel, and thus it may be more effective in diverting seepage to the walls. In contrast, the roughness of the ESF walls may cause asperities that could focus drips. Nonetheless, it demonstrates how seepage could be directed in the tunnels.

8.4 EVALUATING THE ANALOGUES

Although there are many examples of Paleolithic and Neolithic art preserved in caves, questions persist about whether an equal or perhaps even larger number of paintings have been completely destroyed. Null evidence is difficult to evaluate, but a few lines of evidence suggest that paintings have not been totally destroyed in caves where they may have once existed.

First, if paintings had been completely destroyed in some caves, or even parts of caves, one would expect most, if not all, localities to exhibit either a spectrum of preservation from largely destroyed to fully preserved paintings. Alternatively, there should be an explanation for the binary distribution. A variety in the degrees of preservation of cave art was not found in the current literature search, either within individual caves or in the body of literature as a whole. A cave at Palomera in Burgos, Spain, like the cave at Cosquer, has had some paintings removed by water while others are in good condition. This cave, which has paintings dated at 10,950 +/- 100 to 11,540 +/- 100 B.P. (Corchon et al. 1996 [156636], pp. 41–44), has at times had a stream flowing in it that has left organic debris plastered to heights of several meters on the walls. The flooding is younger than the paintings and has apparently destroyed the paintings to the height of the flooding. Lascaux provides another example where one gallery has had over 90% of the paintings removed by wind abrasion (Breisch 1987 [156456], p. 286).

Second, areas where paintings would be least likely to survive, such as drip sites in the ceiling or flow channels on the walls of caves, have probably been the loci of flow for thousands of years. Early man would likely have avoided these areas, because they were too wet to paint. Exceptions to this hypothesis are known. For example, one painting on the ceiling at Chauvet is partly covered by stalactitic calcite (Chauvet et al. 1996 [152249], p. 47). Some paintings have thin coatings of calcite caused by evaporation of thin films of water.

Finally, the sheer number of painted caves and the number of paintings in some of the caves argues for a high degree of preservation. In France and Spain alone, there are more than 150 painted caves (Ruspoli 1987 [156223], p. 18). Grand (1967 [156218], p. 28) reports over 2,188 paintings of animals in 110 caves.

In the case of rock shelters, some observational data correlate with preservation or destruction. In sandstone shelters in India, the roots of banyan trees have been noted to provide a preferential path for water across a painting. The part of the painting exposed to water has been encrusted with calcium deposits, “while leaving another part of the same figure—untouched by water—unscathed” (Neumayer 1983 [156221], p. 6).

Not all underground openings provide appropriate analogues. The previous examples of caves and underground openings were all <100 m from the surface. The Mission Tunnel through the

Santa Ynez Mountains near Santa Barbara, California, is closer in depth (200 to 670 m from the surface) to the potential mined geologic repository (300 m depth), as compared to the previous examples. The Mission Tunnel exhibits rapid response to precipitation events and large amounts of seepage flux (1.23 million m³/yr; Boles 1999 [156635]). Unfortunately, quantitative measurements have not been made, so the percentage of infiltration that becomes seepage is unknown. However, the apparently large amounts of seepage into the Mission Tunnel are caused by flow paths that are within nearly vertical, highly transmissive, fractured sandstone units (Boles 1999 [156635]). Furthermore, at least some part of the flow could be from groundwater seeps below the water table (Boles 1999 [156635]). Thus, the hydrogeology for this potential analogue is drastically different from that for the potential repository at Yucca Mountain, where the hydrologic units are gently dipping and few through-going fractures have a hydrologic connection with the surface.

Mitchell Caverns, located on the eastern slope of the Providence Mountains in the East Mojave National Preserve, California, may also be a potential location for study of seepage. The caverns are found at an elevation of 1,341 m (4,400 ft; Pinto 1989 [156638], p. 6) in a wedge of Permian limestone (approximately 300 Ma; Norris 1999 [156637], p. 10). The limestone layers are upended, folded, and highly fractured by intrusion of younger Jurassic quartz monzonite (approximately 160 Ma; Miller et al. 1991 [156458], Plate 1).

The larger of the caves accessible to the public, Tecopa, exhibits soda straw features, which are hollow stalactites in early stages of development. Tecopa, however, is a drier cave than the other publicly accessible cave, El Pakiva, and is said to be aging. Because Tecopa has two entrances, it is more influenced by the surface environment than El Pakiva cave, which tends to dry out more quickly after a rainfall. Approximately 10 drip locations were observed to begin a few days after a rainfall. All but one of these are in El Pakiva Cave, which is less than 30 m (100 ft) from the surface (Simmons 2002 [157544], pp. 124–125).

The speleothems are nearly inactive under present climate conditions; there are no continuous seeps. The caves respond rapidly after a rainfall. Dripping can be observed to last from a variety of locations up to 28 days after a heavy rainfall (Simmons 2002 [157544], p. 126). Mean annual precipitation measured at the caverns is 18.6 cm (Stein and Warrick 1979 [156642], p. 12).

Because the fractured limestone in which Mitchell Caverns are situated has rapid communication with the ground surface along fracture flow paths after a rainfall, and because there is a considerable bedrock catchment basin above the caves that would induce seepage, they are not an ideal analogue to the conditions expected at Yucca Mountain. Instead, Mitchell Caverns may provide an intermediate analogue between the cave at Altamira, Spain, where very little water has seeped along fractures, and the Mission Tunnel, California, which experiences heavy flow along numerous surface-intersecting pathways.

8.5 SUMMARY OF SEEPAGE ANALOGUES

One important variable for preservation in underground openings is relative humidity. It is obvious that if relative humidity in the drift is kept below 100% by ventilation, then seepage of liquid water would be reduced or completely suppressed. Most caves are close to but below 100% humidity (e.g., Kartchner RH=99.4 % (Buecher 1999 [154295], p. 111); Altamira RH=98

+/- 2% (Breisch 1987 [156456], p. 290; Quindos 1987 [156640], p. 555)). These caves are naturally ventilated; thus, the amount of seepage in these caves would be expected to be low. This would also be true at Yucca Mountain while ventilation is maintained.

This section has examined several different types of qualitative and quantitative natural analogues. The findings support the hypothesis that most of the infiltrating water in the UZ is diverted around underground openings and does not become seepage. The analogues show that this is true even for areas with much greater precipitation rates than that at Yucca Mountain. Although examples exist where large amounts of seepage can be observed (e.g., the Mission Tunnel and Mitchell Caverns), the hydrogeologic setting is significantly different from that at Yucca Mountain, and thus, these are not appropriate analogues. However, for all of the analogues that show some seepage, at least some of the seepage that enters underground openings does not drip, but rather flows down the walls. In the few instances where dripping has been noted in settings that are analogous to Yucca Mountain, the drips can be attributed to asperities in the surface of the roof and ceiling of the opening. Whether water flows on walls or drips depends on conditions affecting drop formation and drop detachment (e.g., surface tension, roughness angle, saturation). Thus, by analogy at Yucca Mountain, although most water would flow around emplacement drifts, the small amount of seepage that would occur would primarily flow down tunnel walls. In the few instances where dripping may occur, it would be expected to be attributable to asperities in the tunnel ceilings.



NOTE: There is no apparent water damage near fractures through both the iron oxide and charcoal portions of the 14,000-year-old painting.

Source: Stuckless 2000 [151957], p. 8.

Figure 8-1. Painted Bison from the Ceiling of the Cave at Altamira, Spain



NOTE: Although there is evidence of water flow down the wall, in general, there is still good preservation.

Source: Chauvet et al. 1996 [152249], Figure 49 (used with permission of the French Ministry of Antiquity).

Figure 8-2. 32,000-year-old Painted Auroches and Horses from Chauvet Cave



NOTE: The tomb shows no evidence of dripping from the ceiling, but plaster on the wall has been damaged by moisture, and some of the paint shows evidence of water running down the wall. The tomb was excavated in limestone about 1,400 B.C.

Source: Simmons 2002 [157544], p. 141.

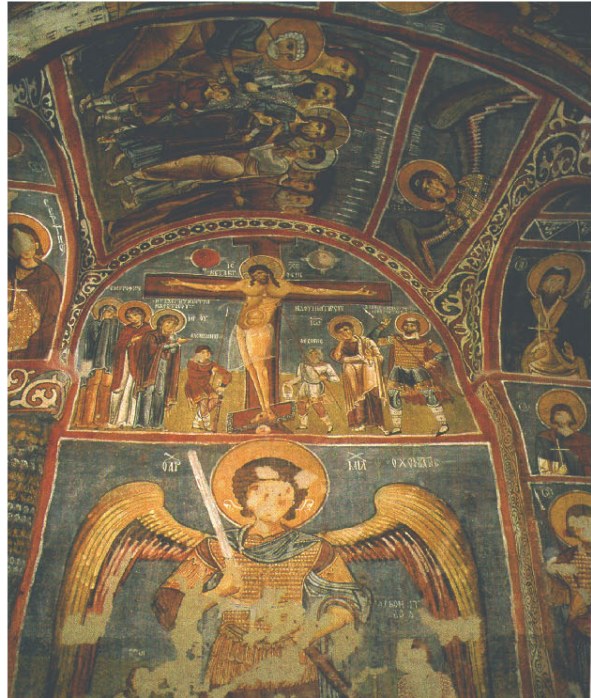
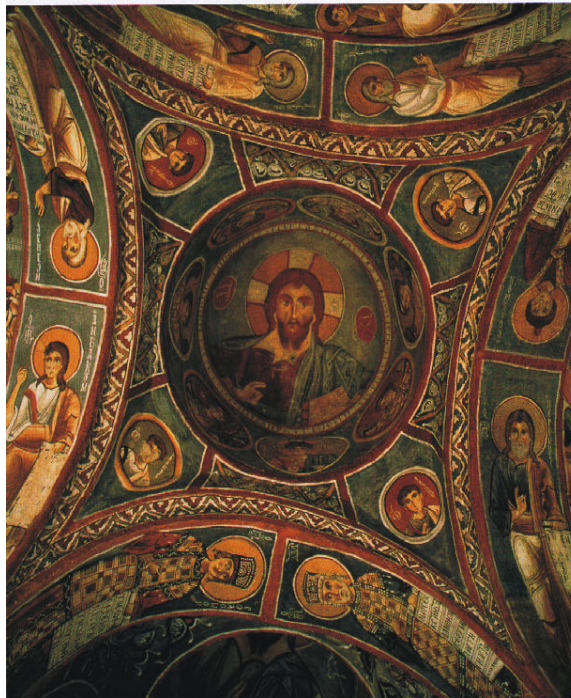
Figure 8-3. The Painted Interior of the Tomb of Sennefer



NOTE: The hexagonal column is from the second century B.C.

Source: Behl 1998 [156213], p. 42.

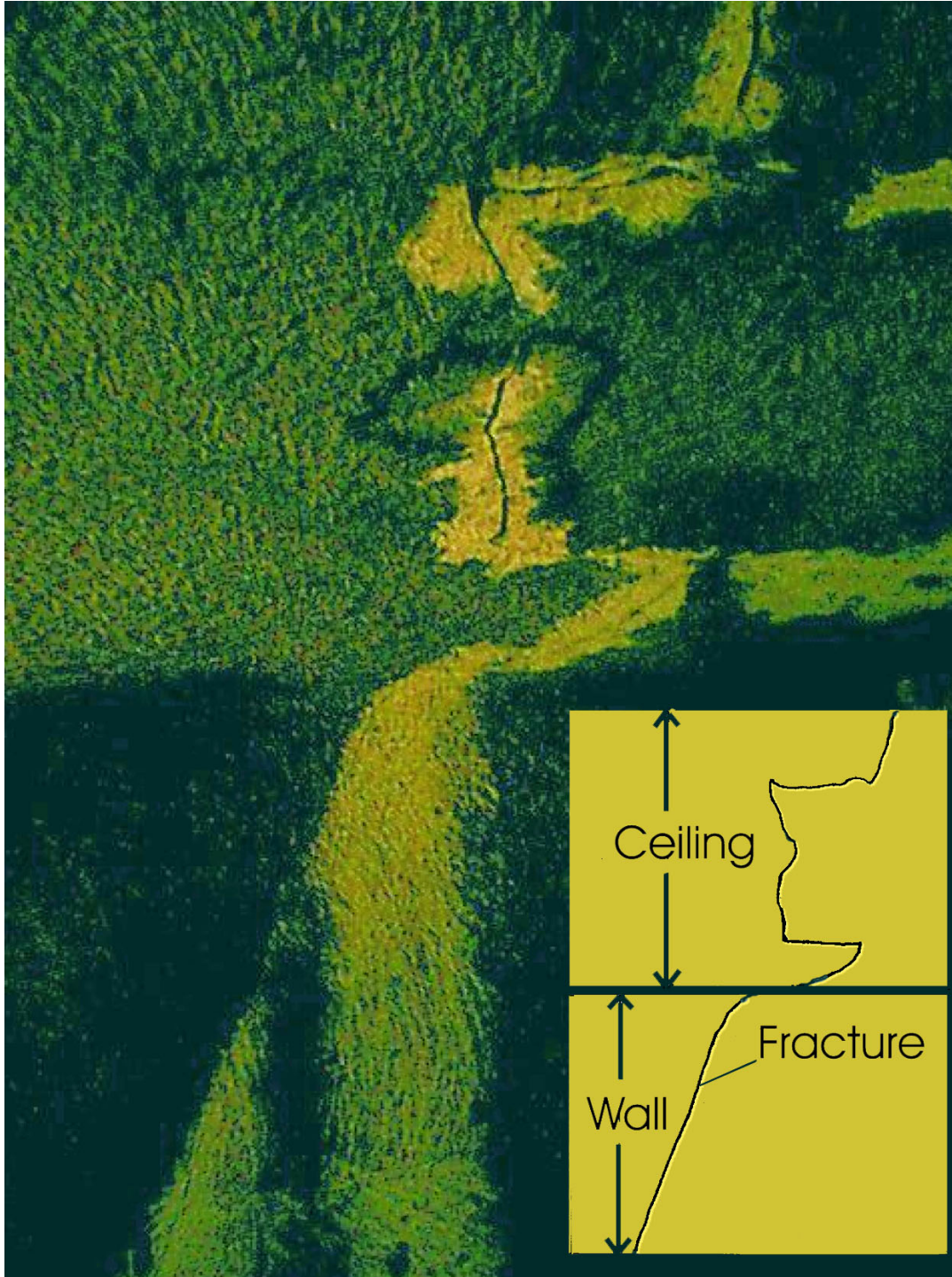
Figure 8-4. Painting from the Underground Ajanta Temple in India Is Fairly Well Preserved in Spite of Its Age and the Wet Climate



NOTE: The perfectly preserved painting on the left was painted in the eleventh century A.D. The painting on the right shows damage from vandals and from spallation of the plaster.

Source: Stuckless 2000 [151957], p. 23.

Figure 8-5. Frescoes on the Ceiling and Walls of the Karanlik Church at Goreme, Turkey, Show Varying Degrees of Preservation, but No Evidence of Dripping from the Ceiling



NOTE: The kitchen was excavated into ash flow tuff and was probably in use until the twelfth century A.D. The soot has been removed adjacent to the fracture in the ceiling, possibly by oxidation. Flow has occurred down the wall, as evidenced by removal of some of the soot below the fracture.

Source: Stuckless 2000 [151957], p. 24.

Figure 8-6. Photograph and Drawing of a Fracture in the Blackened Wall and Ceiling of a Kitchen in a Subterranean Monastery at Goreme, Turkey



NOTE: Water has seeped along joints in the concrete, but rather than dripping, it has flowed along the curvature of the roof.

Source: Simmons 2002 [157544], p. 142.

Figure 8-7. Photograph of Building 810 in the Denver Federal Center, Colorado (a), and Close-up of the Underside of the Roof over the Loading Dock (b)